Use of new generation geospatial data and technology for low cost drought monitoring and SDG reporting solution

A thesis presented in partial fulfillment of the requirement for the degree of

Master of Science
in
Computer Science

at Massey University, Manawatū, New Zealand.

Mohammad Hossain Dehghan-Shoar

2018

Abstract

Food security is dependent on ecosystems including forests, lakes and wetlands, which in turn depend on water availability and quality. The importance of water availability and monitoring drought has been highlighted in the Sustainable Development Goals (SDGs) within the 2030 agenda under indicator 15.3. In this context the UN member countries, which agreed to the SDGs, have an obligation to report their information to the UN. The objective of this research is to develop a methodology to monitor drought and help countries to report their findings to UN in a cost-effective manner.

The Standard Precipitation Index (SPI) is a drought indicator which requires long-term precipitation data collected from weather stations as per World Meteorological Organization recommendation. However, weather stations cannot monitor large areas and many developing countries currently struggling with drought do not have access to a large number of weather-stations due to lack of funds and expertise. Therefore, alternative methodologies should be adopted to monitor SPI.

In this research SPI values were calculated from available weather stations in Iran and New Zealand. By using Google Earth Engine (GEE), Sentinel-1 and Sentinel-2 imagery and other complementary data to estimate SPI values. Two genetic algorithms were created, one which constructed additional features using indices calculated from Sentinel-2 imagery and the other data which was used for feature selection of the Sentinel-2 indices including the constructed features. Followed by the feature selection process two datasets were created which contained the Sentinel-1 and Sentinel-2 data and other complementary information such as seasonal data and Shuttle Radar Topography Mission (SRTM) derived information.

The Automated Machine Learning tool known as TPOT was used to create optimized machine learning pipelines using genetic programming. The resulting models

yielded an average of 90 percent accuracy in 10-fold cross validation for the Sentinel-1 dataset and an average of approximately 70 percent for the Sentinel-2 dataset. The final model achieved a test accuracy of 80 percent in classifying short-term SPI (SPI-1 and SPI-3) and an accuracy of 65 percent of SPI-6 by using the Sentinel-1 test dataset. However, the results generated by using Sentinel-2 dataset was lower than Sentinel-1 (45 percent for SPI-1 and 65 percent for SPI-6) with the exception of SPI-3 which had an accuracy of 85 percent.

The research shows that it is possible to monitor short-term SPI adequately using cost free satellite imagery in particular Sentinel-1 imagery and machine learning. In addition, this methodology reduces the workload on statistical offices of countries in reporting information to the SDG framework for SDG indicator 15.3. It emerged that Sentinel-1 imagery alone cannot be used to monitor SPI and therefore complementary data are required for the monitoring process.

In addition the use of Sentinel-2 imagery did not result in accurate results for SPI-1 and SPI-6 but adequate results for SPI-3. Further research is required to investigate how the use of Sentinel-2 imagery with Sentinel-1 imagery impact the accuracy of the models.

Acknowledgements

I would like to thank my kind supervisors Prof. Hans Guesgen, Dr. Sunil Lal and Dr. Lorenzo De Simone for their guidance and support during my study. In addition I would like to thank my family members for helping me in my time of need in particular my father and mother for their kind support.

Contents

List of Tables

List of Figures

1

Introduction

As the world is experiencing an increase in the occurrence of natural disasters due to the effects of climate change, monitoring and forecasting such events has become ever increasingly important [2]. Drought is a natural disaster which negatively affects people and countries alike.

1.1 Impacts of drought

There are many negative impacts associated with drought. Some of the most important are as follows:

1. Economic: drought affects the industry and business sector of a country resulting in unemployment and overall shrinkage of the economy of a country [3]. Some examples of the economic impacts of drought include:
    (a) Farmers and businesses which require large amounts of water need to spend more money
    (b) The lack of water causes the prices for all products dependent on it to increase
    (c) The loss of crops causes farmers to lose money and smaller farmers to go bankrupt and move to other cities
2. Environmental: animals, humans and vegetation have a large dependency on water and the occurrence of drought causes all of them to suffer [4]. In addition, long term drought may have permanent negative impacts on the environment

such as desertification and extinction of vegetation varieties and wildlife. Some examples of the environmental impacts of drought include:

   (a) The lack of water causes the wildlife and vegetation to suffer
   (b) The long term effect of drought causes desertification of areas which were previously human habitable and causes forced migration
   (c) Drought increases the probability of wildfires due to the lack of moisture in the vegetation and soil [5]

3. Social effects: drought may also have negative effects on public safety and health. Some examples of the social impacts of drought include:

   (a) Drought causes health problems for people [6]
   (b) The scarcity of water causes conflicts for the possession of the remaining water sources [7]

1.2 Types of drought

Generally drought is caused by the reduction of precipitation for an extended period of time and could be associated with other environmental factors such as increase in evaporation, decrease of river discharge and reduction of ground water levels (Figures 1.1, 1.2)[1].

Although the occurrence of drought has been present in the Near East and Africa for a long time [8] the occurrence of this natural disaster has been increasing in other areas such as Europe and New Zealand as well [9, 10]. The National Oceanic and Atmospheric Administration (NOAA) of the United States has defined drought in the following four categories:

1. Meteorological: this type of drought occurs when there are dry weather patterns and there is a reduction in precipitation
2. Hydrological: hydrological drought occurs when there is low water supply and groundwater levels decrease because of long periods of meteorological drought

---

[1] http://drought.unl.edu/Education/DroughtIn-depth/TypesofDrought.aspx

3. Agricultural: agricultural drought occurs when agricultural crops suffer and are under stress from lack of soil moisture

4. Socioeconomic: this type of drought is based on the impacts of the previously stated drought types and causes the suffering of the supply and demand of economic goods

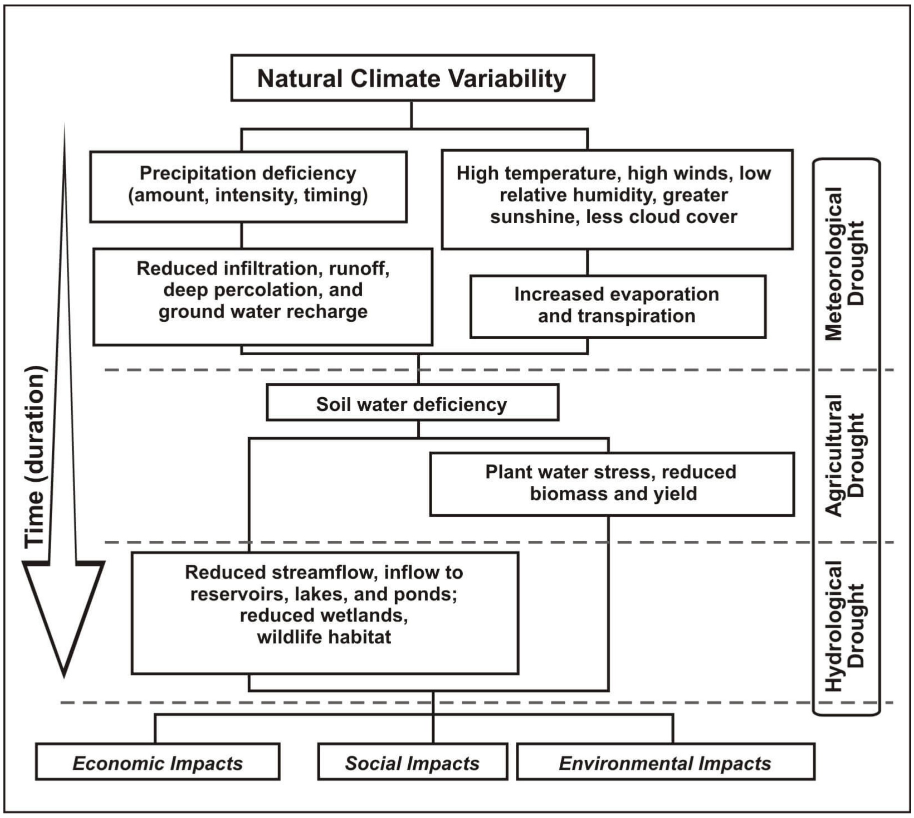

Figure 1.1: Chart displaying different types of droughts and their impacts on the environment

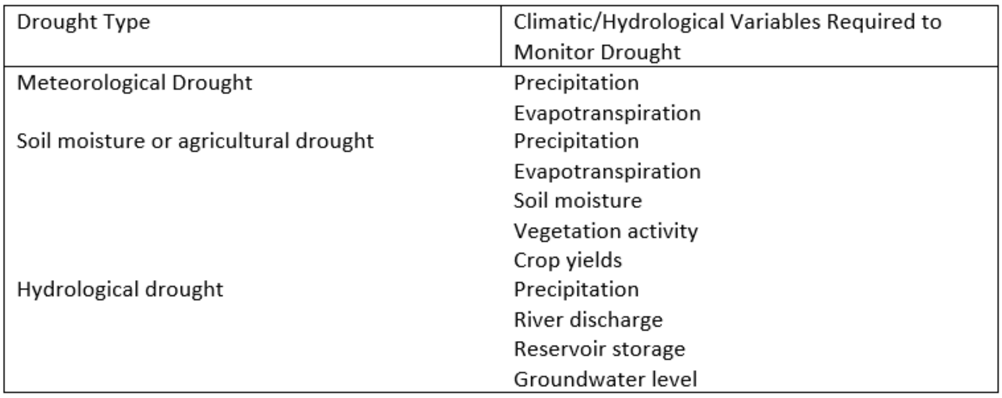

Drought Type	Climatic/Hydrological Variables Required to Monitor Drought
Meteorological Drought	Precipitation Evapotranspiration
Soil moisture or agricultural drought	Precipitation Evapotranspiration Soil moisture Vegetation activity Crop yields
Hydrological drought	Precipitation River discharge Reservoir storage Groundwater level

Figure 1.2: Variables commonly used to monitor different types of drought

1.3 Monitoring drought

While drought can be monitored by using variables seen in Figure 1.2, sometimes gaining access to such data can be difficult for a number of reasons, such as lack of technical skills and funds. As an alternative way to monitor drought, scientists use different types of satellite imagery as they allow monitoring of large areas at a low cost. Different research have been undertaken in order to use hyperspectral and multispectral remote sensing instruments for drought monitoring by using remote sensing indices and spectral bands [11, 12]. A type of satellite (camera) which is very useful for monitoring soil moisture are microwave satellites as the backscatter generated by them is sensitive to soil moisture. However due to the nature of remote sensing instruments they are not as accurate as information collected by using weather stations and cannot be used to measure specific environmental features such as precipitation directly.

It is possible to use both of these monitoring methods, remote sensing and use of weather stations, as inputs to machine learning models which can be used to approximate environmental characteristics such as precipitation or other Ground Truth (GT) data. Furthermore, as satellites revisit an area many times it is possible to create a drought time series. This allows users to monitor drought globally at a low cost, helping the development of sustainable drought management programs, helping to increase food security worldwide and to monitor land degradation trends to fight desertification.

1.4 Objectives

The objectives of this research project are as follows:

1. To develop machine learning models which use remote sensed satellite data (specifically Sentinel-1 and Sentinel-2) to monitor meteorological drought
2. To compare the effectiveness of Sentinel-1 and Sentinel-2 in monitoring meteorological drought

3. To validate the reliability of the developed machine learning models for monitoring meteorological drought by using uncontaminated data

2

Literature Review

2.1 Remote sensing

The field of studying and monitoring an area from a distance by using different instruments such as satellites and Unmanned Aerial Vehicles (UAV) is called remote sensing. This area of study is rapidly evolving as different international organizations such as the National Aeronautics and Space Administration (NASA) and the European Space Agency (ESA) develop and launch new remote sensing instruments. There are two main types of remote sensing satellites [13]:

1. Passive: passive satellites measure the reflected energy from a target area. They do not emit their own energy and use the solar energy coming from the sun (Figure 2.1)[1]

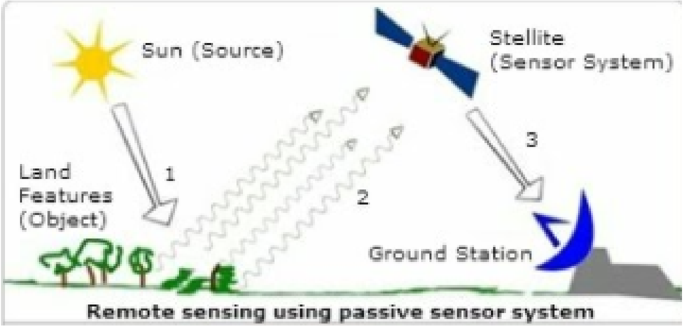

Figure 2.1: Illustration of a passive satellite

2. Active: active satellites emit their own energy to an area and measure the energy reflected by that target area (Figure 2.2)

---

[1] https://sites.google.com/site/tig4un/recursos-de-aprendi/7–active—passive-satellite-sensors

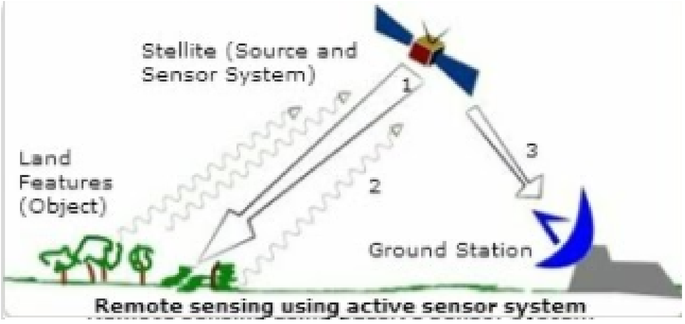

Figure 2.2: Illustration of an active satellite

2.2 Synthetic Aperture Radar (SAR)

An example of a newly developed active remote sensing instrument is the Sentinel-1 Synthetic Aperture Radar (SAR) [14] which is useful for monitoring soil moisture [15], land cover classification and flood monitoring [16]. Sentinel-1 is a C-band instrument with a frequency of 4.20-5.75 GHz and a wave-length of 5.2-7.1 c.m (Table 2.1). However, there are other microwave instruments which use different bands and have different characteristics as well such as PolSar [17].

Table 2.1: Specification of different microwave bands

Band	Frequency (GHz)	Wavelength (cm)
P	0.255-0.390	133-76.9
L	0.390-1.550	76.9-19.3
S	1.550-4.20	19.3-7.1
C	4.20-5.75	7.1-5.2
X	5.75-10.90	5.2-2.7
K	10.90-36.0	2.7-0.83
K_u	10.90-22.0	2.7-1.36
K_a	22.0-36.0	1.36-0.83
Q	36.0-46.0	0.83-0.65
V	46.0-56.0	0.65-0.53
W	56.0-100.0	0.53-0.30

The energy emitted from microwave satellites can pass through clouds and works during day and night. This is particularly useful for areas which are often covered by clouds such as New Zealand. When the energy emitted from the satellite makes contact with different surfaces some of the energy is absorbed while some is reflected. The amount of energy which is reflected can be calculated and is called backscatter. Furthermore, the energy sent to the earth surface are polarized in different ways and the backscatter can be measured (Figure 2.3 and Table 2.2) [2]. Subsequently this can be useful in providing more information about the study area and environmental variables which may be more sensitive to a particular polarization. For example, Bousbih et al [18] has discovered that radar signal strength decreases when vegetation parameters increase when using the Sentinel-1 VV polarization while no vegetation parameter sensitivity is observed in the VH polarization.

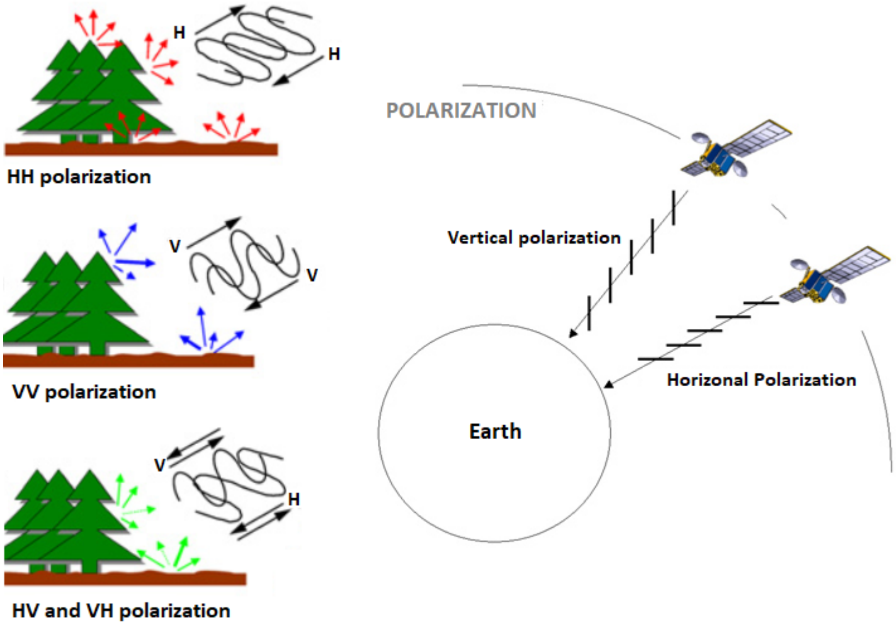

Figure 2.3: Illustration of differently polarized signals interacting with the environment

---

[2] https://sentinel.esa.int/web/sentinel/user-guides/sentinel-1-sar/definitions

Table 2.2: Different types of polarization

Polarization	Description
VV	The energy sent to the surface is vertically polarized and is reflected vertically
HH	The energy sent to the surface is horizontally polarized and is reflected horizontally
HV	The energy sent to the surface is horizontally polarized but reflected vertically
VH	The energy sent to the surface is vertically polarized but reflected horizontally

2.2.1 Microwave imagery and soil moisture

Although more research is required to further understand what polarization types are useful for monitoring soil moisture and drought, there has been evidence which indicates that vertically polarized microwave signals are more sensitive to soil moisture [19]. As there is a strong relationship between drought and low soil moisture [1], by using the backscatter generated from SAR satellite imagery it is possible to monitor soil moisture and drought. The energy reflected from a surface will be different based on the characteristics of an area, as shown in Figure 2.4. Soils with different amounts of water content will have different backscatter values:

1. Dry soil: some of the energy enters the soil while some are reflected
2. Wet soil: more energy is reflected in comparison with dry soil
3. Flooded soil: almost all the energy is reflected

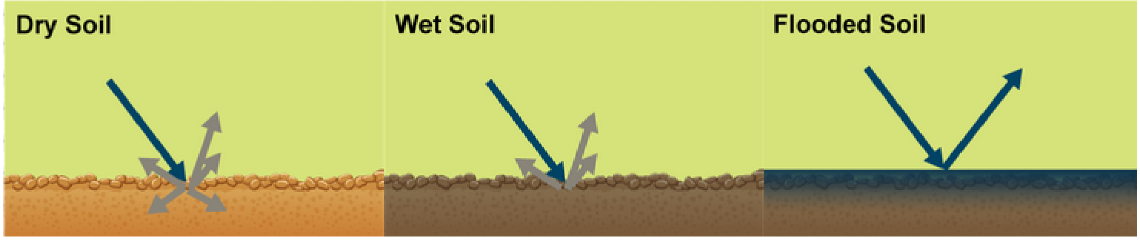

Figure 2.4: Reflection of microwave signals by soils containing different water content

By using this characteristic of SAR imagery it is possible to use backscatter to estimate the amount of water present in the soil and therefore to estimate if there is soil moisture deficit.

2.2.2 Sentinel-1 imagery pre-processing

Sentinel-1 imagery must be pre-processed before the backscatter is calculated. The pre-processing steps are completed by using sophisticated software such as the SENTINEL-1 Toolbox [3]. The pre-processing steps which are commonly undertaken are as follows:

1. Applying the orbit file: in this step the orbit file is used to update the orbit metadata

2. Thermal noise removal: thermal noise removal is used in order to remove the additive noise in sub-swaths. This reduces the discontinuities between sub-swaths for scenes in multi-swath acquisition modes

3. Radiometric calibration: at this stage the backscatter intensity is calculated by using sensor calibration parameters in the GRD (Ground Range Detected) metadata

4. Terrain correction: as the data from ground range geometry does not take into account terrain characteristics, by using SRTM 30 DEM (Digital Elevation Model) or ASTER DEM the ground range geometry is converted to backscatter coefficient (σ°)

5. Conversion of the values to decibels

   $$decibels = 10 \times \log_{10} \sigma^\circ \tag{2.1}$$

   Note that as the backscatter coefficient (σ°) can vary by several orders of magnitude σ° should be recalculated as 10*log10σ°. This formulae measures whether the radiated terrain scatters the incident microwave radiation preferentially away from the SAR or towards the SAR sensor

---

[3] https://developers.google.com/earth-engine/sentinel1

6. The converted values are then transformed to the first and 99th percentiles to preserve the dynamic range against outliers.

2.3 Multispectral satellites (cameras)

Apart from microwave satellites (cameras), multispectral satellites are another type of remote sensing instrument which can be used to monitor geographic areas. Some examples of modern multispectral satellites are:

1. Sentinel-2 [20]
2. Landsat 7 [21]
3. Landsat 8 [22]

Multispectral instruments can have different characteristics such as:

1. Number of bands
2. Resolutions
3. Central wavelengths

For example, although Sentinel-2 has a high resolution, it does not have thermal bands like Landsat 8 and 7 which have a lower resolution in comparison with Sentinel-2 (Table 2.3). Due to this reason it is more suitable to use modern multispectral instruments which provide high resolution imagery as oppose to last generation ones. Different spectral bands have different reactions when they are emitted and reflected by objects present in an area, which helps scientists distinguish and monitor areas of interest [23, 24]. Furthermore, by using the spectral bands different remote sensing indices have been developed, which help scientists monitor vegetation health and other characteristics of areas of interest [25].

Table 2.3: Bands specification for the Sentinel-2 satellite

Sentinel-2 Bands	Central Wavelength (μm)	Resolution (m)
Band 1 – Coastal aerosol	0.443	60
Band 2 – Blue	0.490	10
Band 3 – Green	0.560	10
Band 4 – Red	0.665	10
Band 5 – Vegetation Red Edge	0.705	20
Band 6 – Vegetation Red Edge	0.740	20
Band 7 – Vegetation Red Edge	0.783	20
Band 8 – NIR	0.842	10
Band 8A – Narrow NIR	0.865	20
Band 9 – Water vapour	0.945	60
Band 10 – SWIR – Cirrus	1.375	60
Band 11 – SWIR	1.610	20
Band 12 – SWIR	2.190	20

Although there are many different remote sensing indices developed, the Normalized vegetation Index (NDVI) [26] is the most famous. NDVI is used to monitor the vegetation greenness of a study area hence giving the ability to monitor vegetation health and indirectly attributes related to vegetation health (Figure 2.5). This index is calculated by using the Red and Near Infra Red (NIR) bands of a multi or hyper spectral instruments and can be calculated as seen in equation 2.2.

$$NDVI = \frac{Red - NIR}{Red + NIR} \tag{2.2}$$

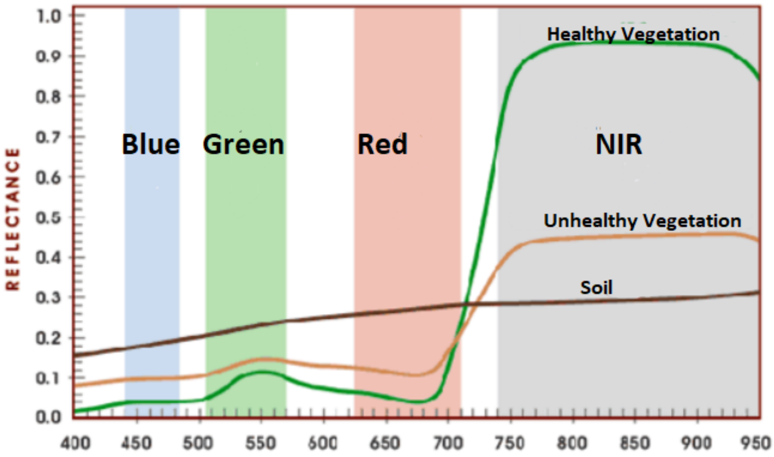

Figure 2.5: Change in reflectance at different wavelengths for various objects

2.3.1 Pre-processing of multispectral imagery

Similar to microwave imagery multispectral imagery also need to be pre-processed before being useful. This is due to the affects of the atmosphere on the incoming energy signals (Figure 2.6)[4]. The unprocessed satellite imagery are represented by digital numbers which demonstrate scaled radiance. Two ways to pre-process multispectral imagery to make them usable are:

1. Top-Of-Atmosphere (TOA) reflectance [27]: this method does not take atmospheric attributes into account which makes it difficult to retrieve actual surface reflectance of an area of interest

2. Land surface reflectance [28]: the surface reflectance of an area of interest is calculated by taking atmospheric characteristics into account and conducting atmospheric correction which provides actual surface reflection. Atmospheric correction removes the scattering and absorption effects caused by the atmosphere. Radiative transfer models and atmospheric modelling are common techniques used for atmospheric correction.

---

[4] https://science.nasa.gov/ems/13_radiationbudget

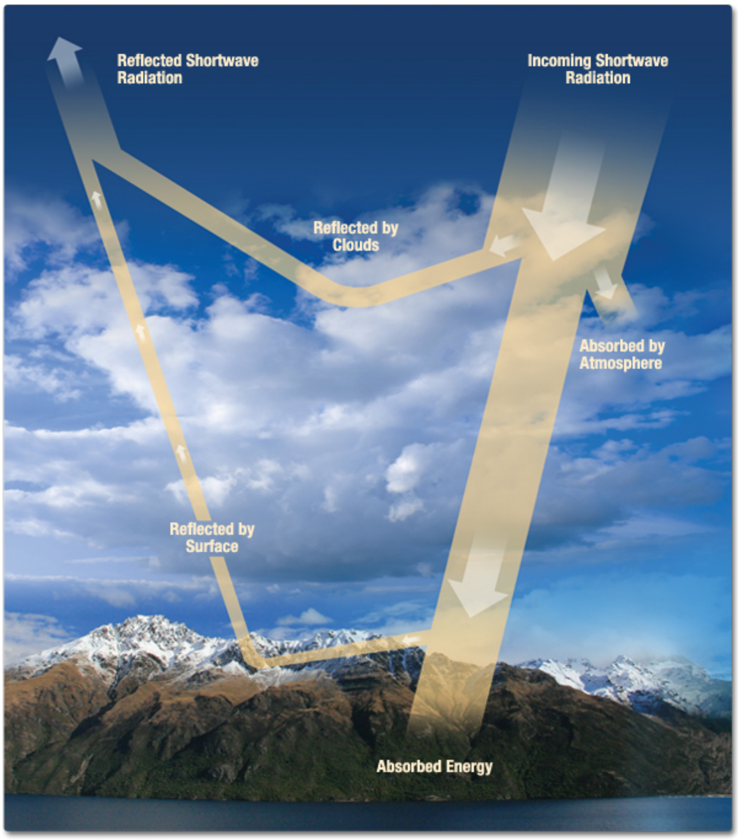

Figure 2.6: Effects of the atmosphere on incoming shortwave radiation

2.4 Cloud computing for remote sensing data

As more remote sensed imagery is captured and made available to the public, users need to download and process these images on their Personal Computers (PC) which is difficult as:

1. The PC requires having access to large amounts of processing power in order to conduct corrections and other required processing tasks to the captured images efficiently. This can be difficult as having access to a PC with high processing capabilities is expensive
2. As more and more imagery is being collected the storage required for these imagery will dramatically increase making it very difficult to store the required imagery locally

As a solution to the stated issues cloud computing platforms are developed which process remote sensed data for users on the cloud making it easy for users to analyze large amounts of remote sensed data easily. Two examples of cloud computing platforms which are popular and are used for processing and downloading remote sensed data are Google Earth Engine (GEE) [29] and Radiant earth [5]. These platforms have large amounts of processing power and provide massive amounts of data to users without requiring large amounts of storage or processing power on the client side. Some datasets offered by the said platforms include Landsat 7 and 8, Sentinel-2, Sentinel-1 and Shuttle Radar Topography Mission (SRTM) [30, 31]. Furthermore they provide easy to use API (Application Programming Interface) for processing and downloading remote sensed imagery which can be used in order to develop various tools. The use of APIs which allow the retrieval and analysis of large amounts of remote sensed data from cloud based services will be very useful for projects such as this where computation power is a constraint.

2.5 Drought indicators

2.5.1 Evapotranspiration

Evapotranspiration [32, 33] is calculated by using information such as evaporation, transpiration and precipitation and gives very useful insight into what is happening in an environment (Figure 2.7). For example as evaporation increases and precipitation decreases for a long period of time there will be a higher likelyhood of a drought occurring. By using Evapotranspiration different drought indicator formulas have been developed to help the drought monitoring process. Two examples of Evapotranspiration based drought indicators are the Aridity Index (AAI) [34] and Moisture Adequacy Index(MAI) [35].

---

[5] https://www.radiant.earth

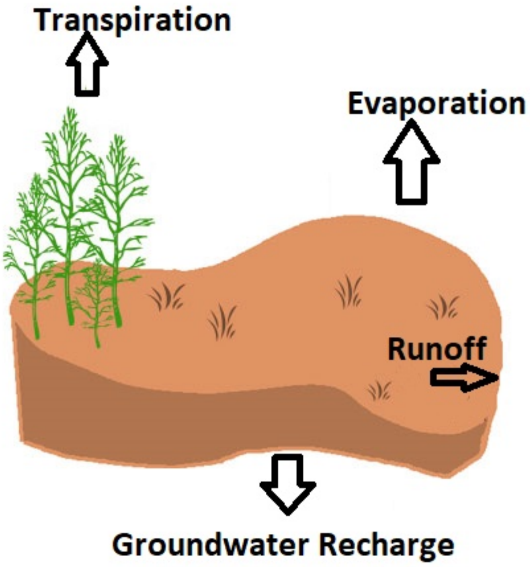

Figure 2.7: A simplified illustration of variables contributing to Evapotranspiration

Although Evapotranspiration is very useful for monitoring the occurrence of drought it requires complex calculations and is very data intensive, therefore it cannot be directly calculated for large areas. However, as precipitation is the most significant attribute affecting the occurrence of droughts, the use of drought indicators based on only precipitation data are popular and widely used [6] [36].

2.5.2 The Standard Precipitation Index

According to the World Meteorological Organization (2012) the Standard Precipitation Index (SPI) [1] is the most common precipitation-based drought indicator used which is very simple to calculate and has been recommended by many organizations such as:

1. The United States National Drought Mitigation Center
2. The World Meteorological Organization
3. The United States National Oceanic and Atmospheric Administration
4. The United States Department of Agriculture

---

[6] http://www.wamis.org/agm/pubs/SPI/WMO1090EN.pdf

5. The United Nations Convention to Combat Desertification

2.5.3 SPI strengths and weaknesses

The main advantages of using SPI are:

1. It is very simple to calculate
2. It only requires precipitation data
3. It can be used for areas with different climates
4. The SPI values calculated in a certain climate can be compared to values calculated for different climates
5. It can be used for monitoring short and long term drought

The main disadvantages of using SPI are:

1. As SPI does not take the temperature of an area into account it cannot be used for monitoring the water balance of an environment
2. Daily precipitation data are required to calculate SPI values

2.5.4 Applications of SPI

Although SPI is useful for monitoring meteorological drought, it can be also used by farmers for choosing the type of crop and the time of plantation in rain-fed croplands in order to make more profit. It has been shown that some crops are sensitive to SPI and can be negatively impacted at certain SPI values [37]. By using the information regarding the sensitivity of different crops to SPI values different applications can be developed which recommend the most suitable crops to plant based on the current and forecasted SPI values. Although there should be a meteorological drought for some time in order for an agricultural drought to occur, research has shown that there is a relationship between remote sensing indices generally associated with agricultural drought such as the Vegetation Health Index (VHI) and SPI values [38] (Figure 2.8). This can provide useful information to farmers for managing their farms.

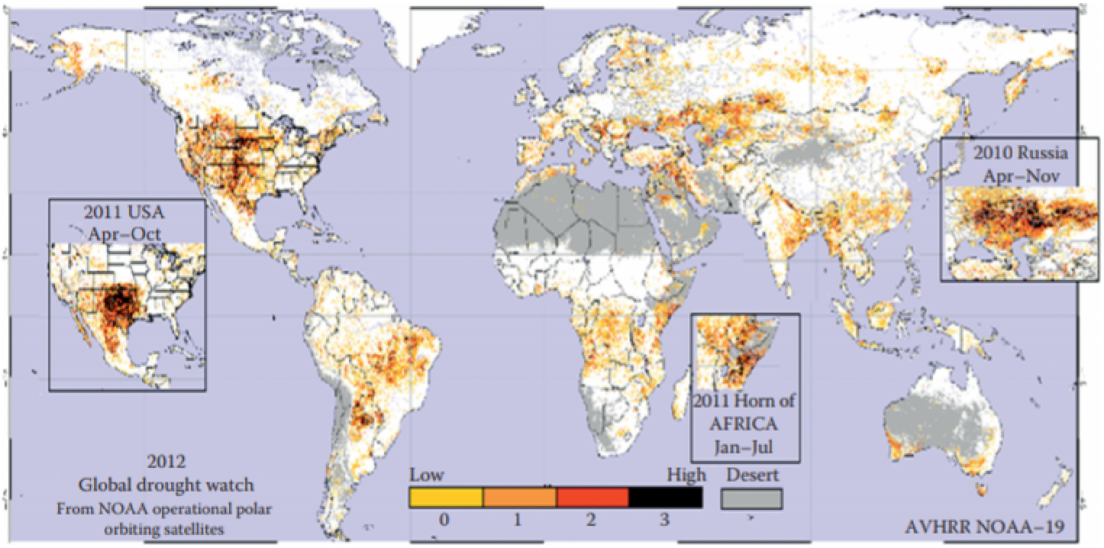

Figure 2.8: Drought occurrence and its intensity derived from VHI

Research has been done to predict SPI values by using remote sensed data. The remote sensed data used in the research undertaken by Park et al (2016) provided information regarding the temperature and precipitation of the study area [39]. Although, the accuracy achieved by using such data was quite high, due to the coarse resolution of the input data the predicted SPI values were coarse as well. Also due to the new release of high resolution and modern remote sensing instruments such as Sentinel-1 and Sentinel-2 there is a lack of research in using these instruments to monitor meteorological drought. In addition, due to the popularity and effectiveness of SPI for monitoring meterological drought comprehensive research is being undertaken using this index for monitoring drought by integrating multi-source remote sensed data [40].

2.5.5 SPI formula

The use of SPI is a very easy method for monitoring meteorological drought. To find SPI values, the difference between the total precipitation in a certain period of time and the long term average precipitation for the same time period is calculated. Furthermore to standardize the SPI values the difference between the total precipitation and long term average precipitation (in a certain time period) is divided by the long-term standard deviation of precipitation for that time period.

$$SPI = \frac{Precipitation\, for\, the\, station - Mean\, precipitation}{Standard\, deviation} \tag{2.3}$$

This indicator can be calculated with different window sizes (number of days). Generally the smaller window sizes are used for indicating short term drought, the larger windows used to indicate long term drought (Table 2.4).

Table 2.4: Different versions of SPI

SPI version	Accumulation of Precipitation
SPI-1	1 month
SPI-3	3 month
SPI-6	6 month
SPI-12	12 month
SPI-24	24 month

In order to help monitor drought severity by using SPI, McKee (1993) [1] developed labels depicting drought severity based on SPI values as seen in Table 2.5

Table 2.5: Different SPI values and their labels

SPI value	Classification
Greater than 0	No drought
0 to -0.99	Mild drought
-1 to -1.49	Moderate drought
-1.50 to -1.99	Severe drought
-2 or less	Extreme drought

2.6 Machine learning

By having access to modern high resolution satellite imagery and using the advancements in the field of machine learning, many researchers have used remote sensed data as input variables with various machine learning algorithms to approximate target values [41, 42, 43]. For example, it is important for decision makers and scientists to know information about soil properties before investing and starting large agricultural projects. This is because certain crops are sensitive to soil contents such as pH and salinity levels. Traditionally, soil is tested using sophisticated laboratories to find such information. However, this process can be time consuming, difficult and expensive.

To overcome this issue, it is possible to use satellite imagery or other remote sensing instruments and machine learning to estimate various soil properties. Hengl et al (2017) has used remote sensing data from SRTM, Moderate Resolution Imaging Spectroradiometer (MODIS) and other instruments with different machine learning algorithms to predict soil properties such as organic carbon, bulk density and pH successfully. In addition, Marj and Meijerink (2011) have used the well-known remote sensing index called NDVI and ANN (Artificial Neural Networks) to forecast agricultural drought with a high accuracy.

However, as the field of machine learning is advancing and new satellites such as Sentinel-1 and Sentinel-2 are launched into orbit more research is required to see how to further improve the drought monitoring and forecasting process. In addition, Artificial Neural Networks (ANN) and Ensemble Algorithms are some of the more popular algorithms which have been used with remote sensed data for drought monitoring.

2.6.1 The Artificial Neuron

An Artificial Neuron (AN) [44] is loosely based on the biological neurons in human and animal brains (Figure 2.9). Each neuron by itself can be a classifier but a very simple one with limitations. The neuron has an activation node which takes previous data and generates a weighted sum which is sent to an activation function in order to calculate an output. Furthermore, an AN also has a bias neuron as well which allows the curve of the activation function (Figure 2.10) to be shifted to the left or right.

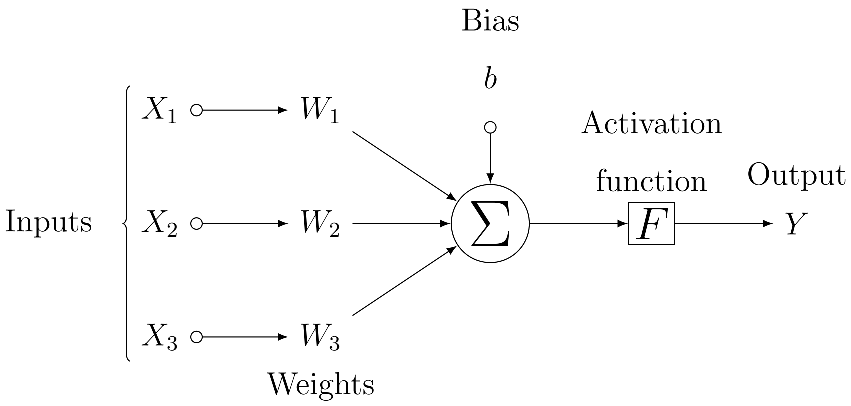

Figure 2.9: Illustration of an Artificial Neuron

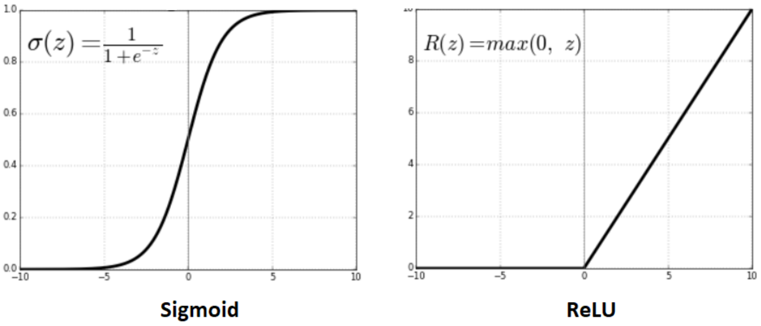

Figure 2.10: Illustration of the Sigmoid and ReLU activation functions

2.6.2 Artificial Neural Networks

It is possible to connect many Artificial Neurons together to create an Artificial Neural Network (ANN) [45], which could solve complex problems. An ANN (Figure 2.11) is constructed of a number of different layers. These layers, which contain artificial neurons, perform transformations on the input data received from previous neurons and conduct their own transformation and send the transformed data to the next neuron in the next layer until an output is produced. The layers of an ANN are:

1. Input layer: the number of neurons available in the input layer determines how many input values (features) can enter each neuron

2. Hidden layers: the hidden layers in an ANN can apply any function to the previous layer hence transforming the inputs. Having a number of hidden

layers can be very useful when an ANN is trying to solve complex problems such as image recognition

3. Output layer: at this layer of an ANN solutions to the problem which the ANN was solving will be produced. The number of neurons present in this layer are determined by the number of possible solutions

An important aspect of ANN is how they undertake the learning process. An ANN has a system of weighted interconnections which are modified during the learning process. Initially the weights of the interconnections are generated randomly however, to improve the performance of the ANN these weighted connections should be readjusted and optimized. The learning rule is used to adjust the weights of the connections to improve the performance of the ANN and help it learn. The delta rule is the most common learning rule used in ANN and is often used with a type of ANN known as the backpropagation neural network (Figure 2.11).

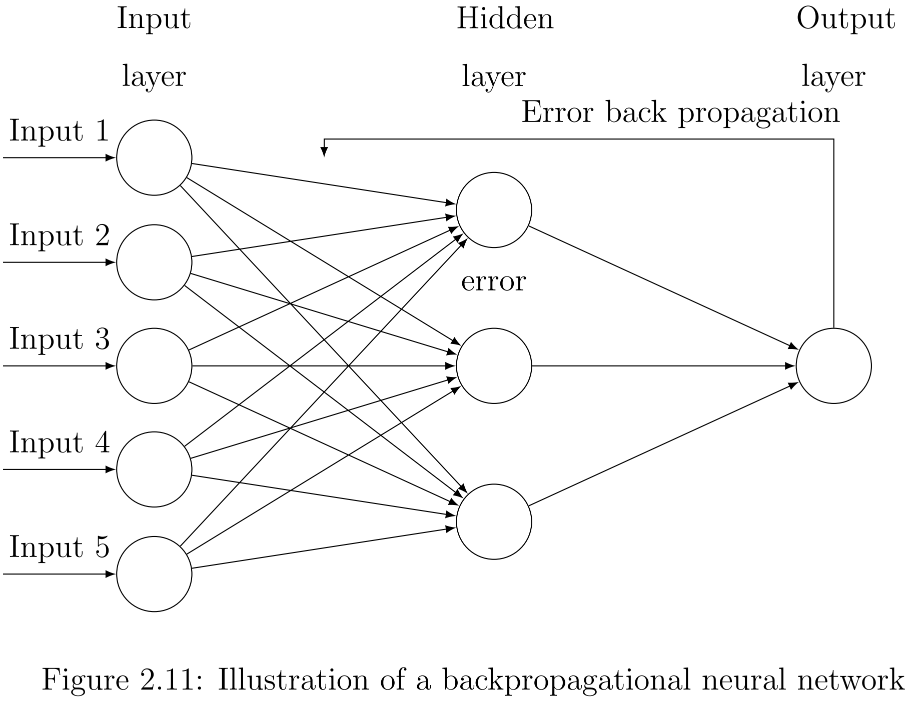

Figure 2.11: Illustration of a backpropagational neural network

Backpropagation or backward propagation of errors is a technique used in ANN to calculate a gradient needed for the adjustment of the weights used in the network. The error is computed throughout all the ANN layers. Backpropagation is a generalization of the delta rule to ANN which is made possible by using the chain rule to successively calculate gradients for each layer of the ANN. Backpropagation is often used by the gradient descent (Figure 2.12) optimization algorithm in order to adjust the weight of neurons by calculating the gradient of the loss function.

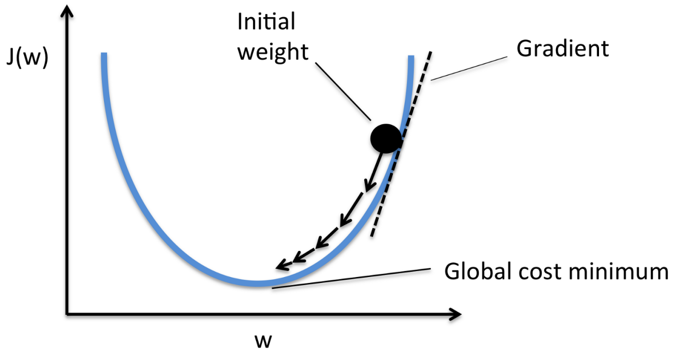

Figure 2.12: Illustration of Gradient Descent

2.6.3 Ensemble Machine Learning Algorithms

Ensemble learning methods are used to create and combine several machine learning techniques into a single predictive model to decrease variance, bias and improve predictions (Figure 2.13). Other applications of Ensemble learning methods are:

1. Selecting optimal features
2. Data fusion

Ensemble learning methods can be divided into two categories:

1. Sequential ensemble methods: the base learners for this type of ensemble method are generated sequentially [46]
2. Parallel ensemble methods: the base learners for this type of ensemble method are generated in parallel [47]

Most ensemble learners use a single base learning algorithm to produce homogeneous base learners which lead to homogeneous ensembles. However, there are some methods which use heterogeneous learners leading to heterogeneous ensembles [48]. For ensemble learning methods to be more effective than any of their individual members, the base learners created should be diverse. Some examples of commonly used ensemble algorithms are:

1. Bagging (parallel ensemble method): bagging or Bootstrap aggregating is an ensemble meta algorithm which improves the accuracy of machine learning algorithms by combining the predictions from multiple algorithms together in order to improve the overall accuracy of the model. An example of an algorithm which uses bagging is the Random Forest algorithm [49, 50]

2. Boosting (sequential ensemble method): these types of algorithms try to create and combine multiple weak learners into a strong learner. Weak learners can be described as a classifier which has a low correlation with the actual classification while a strong learner is a classifier which is highly correlated with the true classification. An example of an algorithm which uses boosting methods is the Gradient Boosting Classifier [51]. Boosting algorithms fit a sequence of weak learners to weighted versions of the data. Extra weight is given to samples that were misclassified by the classifier earlier. The predictions are combined through weighted majority voting (Figure 2.13) or a weighted sum to produce a final result.

The main difference between boosting and bagging methods is that boosting algorithms are trained sequentially and bagging methods are trained in parallel.

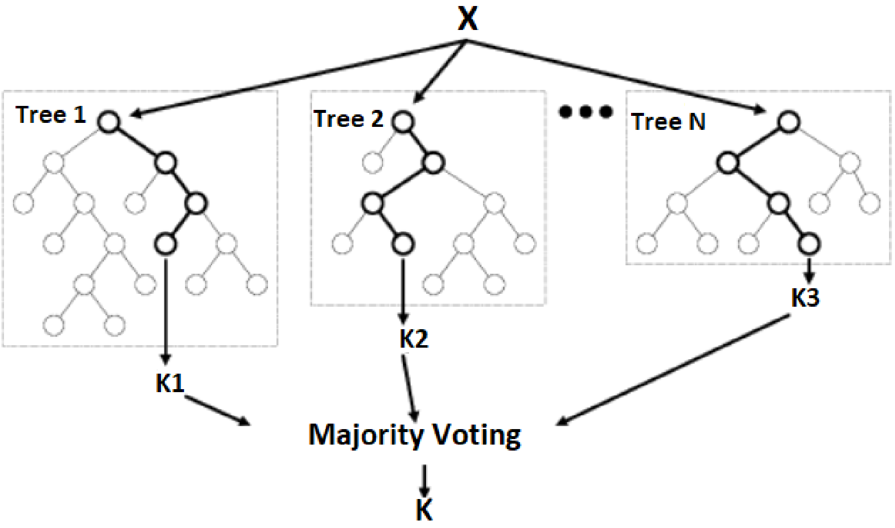

Figure 2.13: Combining the results from different learners by using majority voting to achieve a final solution

Other important aspects of ensemble algorithms include:

1. Max depth: the size of each estimator (tree) can be controlled by setting the tree depth (Figure 2.14)

2. Learning rate : learning rate is a hyper-parameter in the range (0.0, 1.0) that controls over-fitting via shrinkage [52]

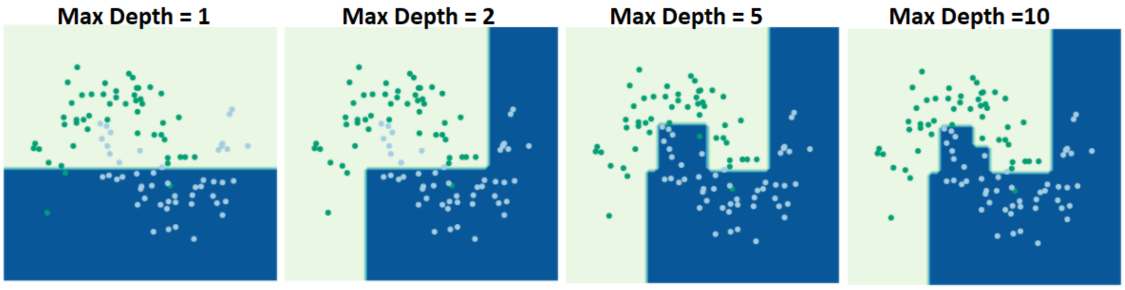

Figure 2.14: Demonstration of the effect of max depth for a classification problem

In addition, ensemble machine learning algorithms have been used for monitoring SPI by means of using coarse remote sensing imagery [39]. There is a lack of research in using new multispectral and microwave satellite imagery such as Sentinel-1 and Sentinel-2 in monitoring drought. This can be due to the advances in the field of remote sensing and deployment of new remote sensing instruments. Therefore, it is necessary to evaluate the performance of ensemble algorithms to predict drought by using high-resolution and modern remote sensing instruments.

2.6.4 The issue of overfitting

One goal of machine learning is to develop models which can describe a target function accurately. The models are created from input data by using inductive learning. The developed models should be able to generalize the learned concepts in order to perform well when trying to find a solution for data not included in the training process of the model. Machine learning models are generally created and tested by using the following different datasets:

1. Training dataset: data used for creating the model

2. Validation dataset: uncontaminated data not included in the testing and training datasets which is used to validate the performance of the model

3. Testing dataset: data used for testing the accuracy of the trained model

A model is said to be suffering from over-fitting when it is trained perfectly on the training dataset but performs poorly on the test dataset. On the other hand when the model performs poorly on both the training, testing and validation datasets it is a sign of underfitting. Overfitting or underfitting can reflect the complexity of a model with respect to the data it is being trained on. Therefore, overfitting or underfitting can be summarized as follows:

1. Overfitting occurs when a model captures the noise of the dataset and fits the data too well. Overfitting also occurs if the model shows low bias but high variance

2. Underfitting occurs when a model cannot capture the generalized trend of the dataset and does not fit the data well enough. Underfitting also occurs if the model shows low variance but high bias

2.6.5 Curse of Dimensionality

Machine learning algorithms require data that can be used to approximate target values successfully. However if the number of features in the input data increases beyond a certain level, the performance of the algorithms will decrease. This is called the curse of dimensionality which refers to how certain learning algorithms may perform poorly with high-dimensional data. This term was first stated by Bellman in his book on dynamic programming [53] and Adaptive Control Processes [54]. For example, assuming that an object has been lost on a straight line one can simply search the 1-dimensional line to find the lost object with no problem. However, if an object is placed in a 2-dimensional square it becomes much harder to find the lost object. As the number of dimensions in the search space increases it becomes more difficult to find the lost object.

As seen in Figure 2.15 as the dimensions of a search space increases the positions where the object might be located at also increases. For example, assuming that the object in the straight line in Figure 2.15 can be located in 10 possible locations compared to 1000 possible positions in 3 dimensional space (Table 2.6). Therefore, as the number of features in a dataset increases more samples are required to help mitigate the curse of dimensionality. As a rule of thumb, for the number of features (n) present in a dataset 2^n samples should be available.

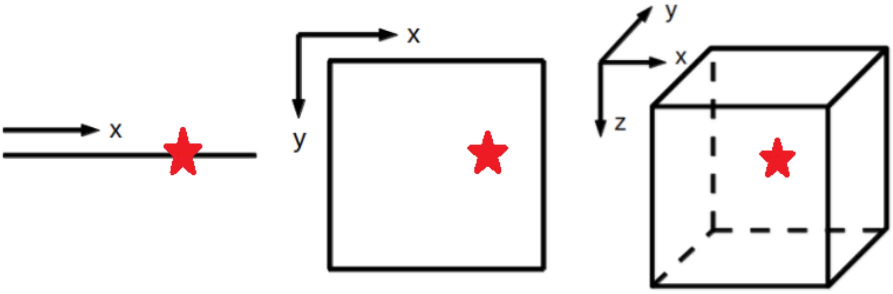

Figure 2.15: Illustration of an object present in a search space with different dimensions

Table 2.6: Possible locations of the object in one, two and three dimensions

Shapes	Possible positions
line (1-Dimension)	10
square (2-Dimension)	$10 \times 10 = 100$
cube (3-Dimension)	$10 \times 10 \times 10 = 1000$

Different approaches have been developed to overcome the curse of dimensionality such as:

1. Principal Component Analysis (PCA): a famous dimensionality reduction method that yields uncorrelated, linear combinations of the original data. PCA tries to find a linear subspace of lower dimensionality [55]

2. Feature selection techniques: feature selection techniques try to find the most useful features (data) in the dataset which improve the performance of model while removing the feature which do not improve the models accuracy hence reducing the dimensionality of the dataset [56]

2.6.6 Genetic algorithms for feature selection and model optimization

Genetic algorithms are often used to conduct feature selection and elimination of unnecessary input data while maintaining or improving the accuracy of machine learning models [57]. Genetic algorithms have also been used to reduce the dimensionality of remote sensed data [58].

In order to find the best solution in a search space by using genetic algorithms, it is necessary to run the algorithm for multiple generations. Furthermore, it is also necessary to repeat the search process by using the genetic algorithm multiple times in-order to have a better chance in finding the best solution (global maximum) in the search space (Figure 2.16).

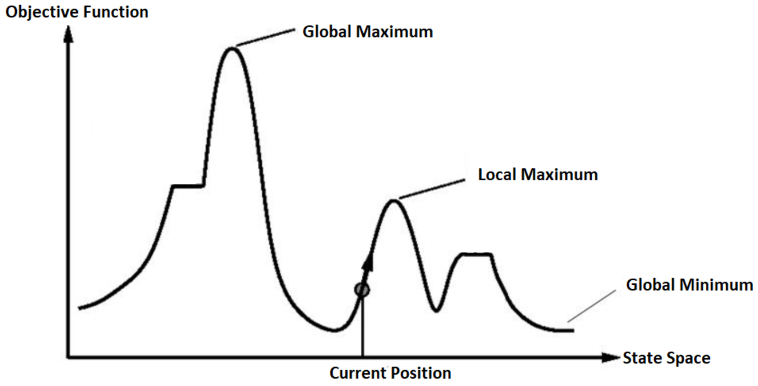

Figure 2.16: Illustration of a search space and the global maximum

As shown in Figure 2.18 a genetic algorithm consists of the following aspects:

1. Initialize population: a population is a subset of solutions in the current generation made up of genes and chromosomes. It can also be defined as a set of chromosomes (Figure 2.17)
2. Evaluate fitness: the fitness function takes a candidate solution of the problem at hand as input and determines the quality of the solution
3. Stop condition: if the stop condition is satisfied the genetic algorithm will stop and a final solution is generated

4. Selection: if the stop condition is not met the selection policy determines which individuals should be removed and which individuals should be kept and used in the next generation of the genetic algorithm

5. Cross over and mutation: the selected parents (individuals) create new offspring (individuals) by performing a crossover operation on chromosomes. Furthermore by allowing a small probability of mutation in the genes in the chromosomes, genetic diversity is introduced which allows the possibility of finding a better solution

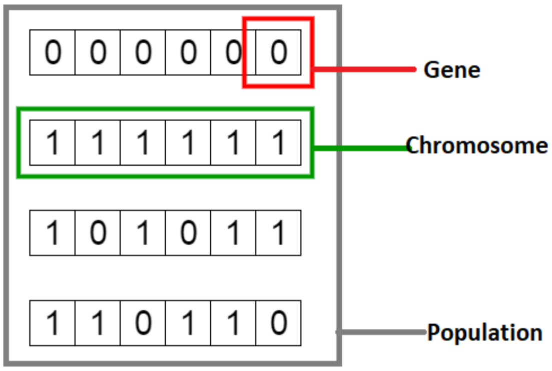

Figure 2.17: Illustration of Population, Chromosomes and Genes in genetic algorithms

6. Output result: after the stop condition is satisfied a final improved solution is created

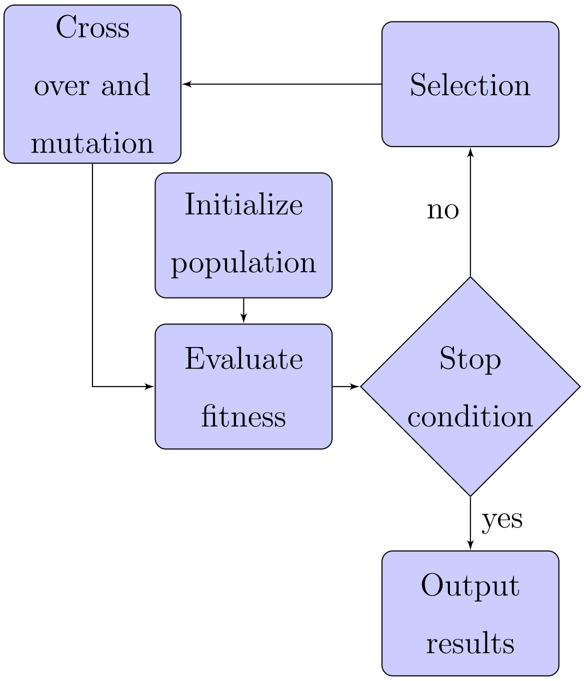

Figure 2.18: Flowchart of a genetic algorithm

Other than using them for model optimization [59], genetic algorithms can be used for feature selection. To use a genetic algorithm for feature selection, the individuals chosen by the genetic algorithm are subsets of the features in the dataset. The features are encoded in binary which allows the genetic algorithm to select some while excluding others. The fitness value of the subset of the features selected is measured by using root-mean-square error (RMSE) or classification accuracy. This process will be repeated by selecting different subsets of features from the dataset while excluding some until an end condition is met. Finally, features which resulted in the highest fitness values are selected and can be used in a new dataset.

Although the use of feature selection and other dimension reduction techniques such as PCA can both be used for reducing the dimension of datasets, using feature selection techniques are more suitable for processing very large images. This is due to the fact that it is very difficult to conduct dimension reduction techniques (such as PCA) on very large images because of memory constraints and the fact that it is common practise to process large images in chunks.

3

Materials and Methods

The chosen drought indicators for this research project were SPI-1, SPI-3 and SPI-6 (Table 2.4). The precipitation data was collected and used from weather stations in provinces of Kermanshah, North Khorasan and Hamedan in Iran for the years 1960 to 2016 (Figure 3.1). In addition, precipitation data for weather stations located in the Palmerston North and Canterbury regions of New Zealand for the years 1980 to 2018 were acquired by using the national climate database created by the National Institute of Water and Atmospheric Research (NIWA) of New Zealand (Figure 3.2) [1].

The Kermanshah and North Khorasan provinces of Iran are located in the mountainous regions of Iran where the climate is warm and dry but at higher altitudes and near the mountain peaks the climate is semi-humid and cold. These provinces also have a cold climate on high altitudes with very long winters. Unlike Kermanshah and North Khorasan the Hamedan province has a moderate cold climate and is located near the Zagros mountain range. Hamedan has a lower temperature and more severe winters in comparison with North Khorasan and Kermanshah [60].

Unlike Iran which has very diverse climates throughout the country (although most of the country is arid or semi-arid), most of New Zealand has mild temperatures and high amounts of precipitation. However, according to NIWA there are some differences in the climates in New Zealand [2].

---

[1] https://cliflo.niwa.co.nz

[2] https://www.niwa.co.nz/education-and-training/schools/resources/climate/overview

The collected daily precipitation data was then used to calculate daily SPI-1, SPI-3 and SPI-6 based on the R SPEI package [61, 62]. The calculated SPI values were labeled by using the Mckee et al (1993) labeling scheme (Table 3.1) and were added to the datasets as GT (Ground Truth) data.

Table 3.1: Different SPI values and their classifications scheme based on Mckee (1993) [1]

SPI value	Classification	Label in the dataset
Greater than 0	No drought	5
0 do -0.99	Mild drought	4
-1 do -1.49	Moderate drought	3
-1.50 do -1.99	Severe drought	2
-2 or less	Extreme drought	1

Followed by the calculation of the SPI values by using precipitation data collected from weather stations in Iran and New Zealand, two datasets were created for training and testing purposes. The testing dataset consisted of weather stations not present in the training dataset. This was intended to provide a way to measure the accuracy of the developed models for geographical data and areas which were not included in the training dataset. The weather stations used for creating the models can be seen in Table 3.2 and the weather stations used for testing the models can be seen in Table 3.3.

Figure 3.1: The locations of the weather stations used from Iran

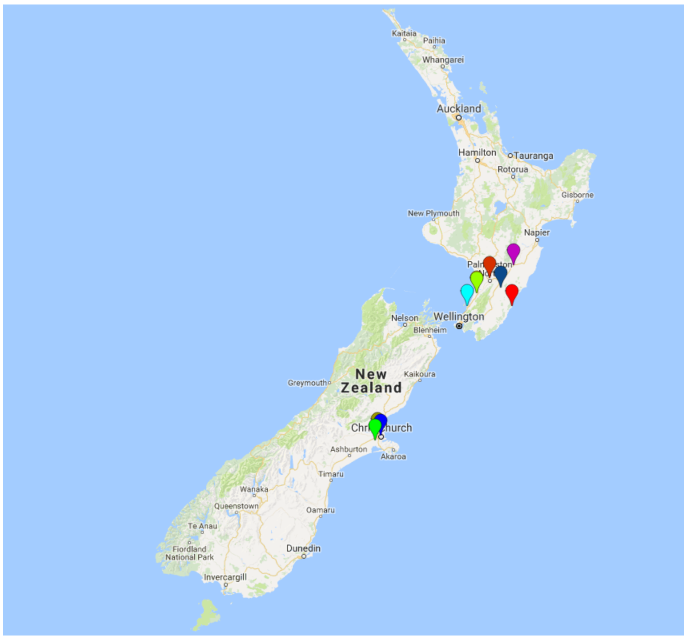

Figure 3.2: The locations of the weather stations used from New Zealand

Table 3.2: List of weather stations used for creating the models

Weather Station Name	Weather Station Location (Latitude,Longitude)
Qasreshirin	45.6,34.53
kermanshah	47.12,34.28
Kangavar	48,34.5
EslamabadeGharb	46.43,34.13
Bojnurd	57.303333,37.486944
Raz	57.101389,37.93972
Farouj	58.226667,37.22083
Maneh	56.945278,37.56527
Esfarayen	57.494722,37.048889
Jajarm	56.338056,36.96194
Hamedan Airport	48.53,34.87
Malayer	48.85,34.25
Nahavand	48.42,34.15
Pahiatua Ews	-40.50652, 175.91586
Levin Ews	-40.62699,175.26193
Levin Aws	-40.622 ,175.257
Takapau Plains Aws	-40.043 ,176.268
Wanganui Aws	-39.962, 175.024
Lincoln, Broadfield Ews	-43.62622,172.4704
Christchurch, Kyle St Ews	-43.53074, 172.60769
Ravansar	46.67,34.72

Table 3.3: List of weather stations used for testing the models

Weather Station Name	Weather Station Location (Latitude,Longitude)
Shirvan	57.8375,37.43444
Asadabad	48.12,34.77
Sonqor	47.58,34.78
Palmerston North Aws	-40.31858,175.61459
Castlepoint Aws	-40.90417, 176.2118
Paraparaumu Ews	-40.90392, 174.98437
Christchurch Aero	-43.493, 172.537

Because some weather stations were located in the urban areas and due to the fact that the Sentinel-1 satellite is very sensitive to artificial surfaces, the location where the satellite imagery were retrieved from was moved to the closest non-urban area within 200 metres for multiple study areas.

Followed by the calculation of the different SPI values, the satellite imagery (Sentinel-1, Sentinel-2 and SRTM) for the stated geographical locations (weather stations) were collected by using GEE and added to the datasets alongside the SPI values. Only the satellite imagery which were captured on the same date as the calculated SPI values were used in the datasets and the remaining SPI values were discarded. For each satellite (Sentinel-1 and Sentinel-2) three different models were created which classified SPI-1, SPI-3 and SPI-6. The methodologies used for creating the models are as follows:

3.1 Sentinel-2 methodology

The Sentinel-2 satellite imagery were retrieved by using the GEE Python API. The images with the highest quality and least cloud cover were selected for locations where the weather stations were present. In addition, the pixel at the weather station location was identified and the contiguous pixels were considered within a 45 metres buffer (9 pixels). Finally the values for all pixels present in the circular buffer were averaged (Figure 3.3). This procedure was undertaken to ensure that the satellite imagery represented the GT more accurately.

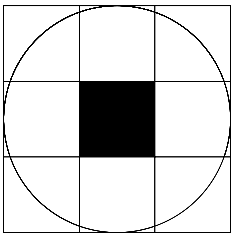

Figure 3.3: Circular buffer created and used to extract eight pixels surrounding the weather station. The black pixel represents the weather station location

Although GEE provides free access to Sentinel-2 imagery, the Sentinel-2 imagery available is in TOA format (see section 2.3.1) which does not represent actual surface reflectance. Therefore, the acquired TOA imagery were converted to surface reflectance by using the open source Python based atmospheric correction tool 6S emulator which is based on the 6S radiative transfer model [63][64]. This tool uses Interpolated Look Up Tables (LUT) to convert Sentinel-2 TOA imagery to Sentinel-2 land surface reflectance imagery. The LUT were used to calculate atmospheric correction coefficients A and B to convert at-sensor radiance to surface reflectance.

To calculate these coefficients the following inputs were used:

1. Solar zentith
2. Water vapour
3. Ozone [cm-atm]
4. Aerosol optical thickness
5. Surface altitude

The LUT were created at perihelion (Figure 3.4) and the Earth Elliptical Orbit was calculated using equation 3.1. In addition, new values of A and B were calculated by multiplying them by the Earth Elliptical Orbit value.

$$EEO = 0.03275104 \times cos(\frac{Day\ of\ year}{59.66638337}) + 0.96804905 \tag{3.1}$$

Finally the surface reflectance was calculated by using equation 3.2.

$$Surface\,reflectance = \frac{Sensor\,radiance - A}{B} \tag{3.2}$$

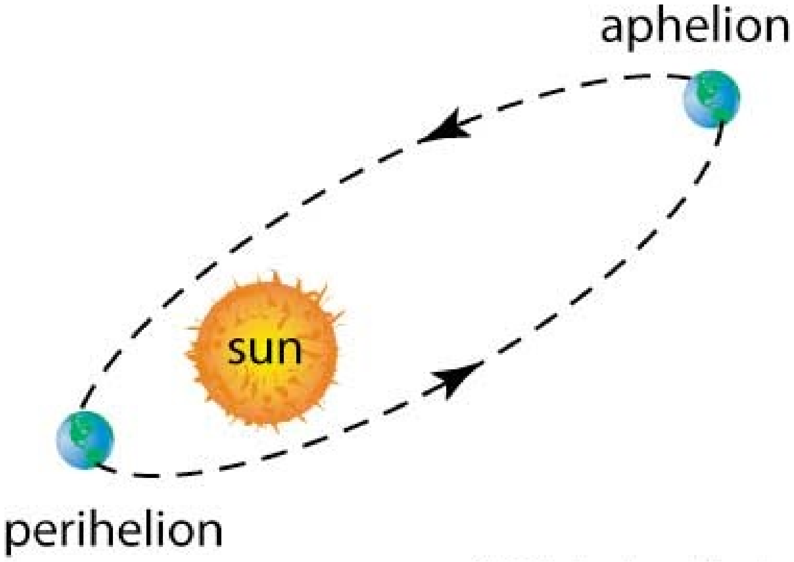

Figure 3.4: Depiction of earth at perihelion and aphelion

Followed by the calculation of the surface reflectance of Sentinel-2 imagery for the desired areas, the spectral bands illustrated in Table 3.4 were saved as an Excel document.

Table 3.4: Atmospherically corrected bands retrieved from Sentinel-2

Retrieved Sentinel-2 corrected bands	
Red	R
Green	G
Blue	B
Near Infra Red	NIR
Short Wave Infrared 1	SWIR-1
Short Wave Infrared 2	SWIR-2

Based on the literature review undertaken, different remote sensing indices which were related to drought were calculated by using the corrected Sentinel-2 bands. The list of the calculated indices can be seen in Table 3.5. It is to be mentioned that although some of the indices seen in Table 3.5 are designed for other satellites, the most similar Sentinel-2 bands with the closest central wavelength to the original have been used instead. More information regarding the indices stated in Table 3.5 can be found in the cited literature and by using the Index DataBase (IDB) website [3].

Table 3.5: Remote sensing indices calculated by using the Sentinel-2 spectral bands

Index name	Acronym
Normalized Difference Vegetation Index	NDVI
Modified Simple Ratio [65]	MSR (SWIR-1 and NIR)
Land Surface Water Index [66]	LSWI
Surface Water Capacity Index [67]	SWCI
Visible and Shortwave Infrared Drought Index [68]	VSDI
Normalized Difference Water Index [69]	NDWI
Modified Photochemical Reflectance Index [70]	MPRI
Normalized Difference Drought Index [71]	NDDI
Moisture Stress Index [72]	MSI
Global Vegetation Moisture Index [73]	GVMI
Chlorophyll Index Green [74]	
Normalized Multi-band Drought Index [71]	NMDI
Tasseled Cap wetness [75]	
Green-Red Vegetation Index [76]	GRVI
Difference Vegetation Index [77]	DVI
Difference Water Index [78]	DWI
Difference Drought Index [78]	DDI
Moisture Adjusted Vegetation Index [79]	MAVI
Modified Normalized Difference Vegetation Index [80]	MNDVI
Enhanced Vegetation Index [81]	EVI
Tasseled Cap greenness [82]	
Specific Leaf Area Vegetation Index [83]	SLAVI

---

[3] https://www.indexdatabase.de

Reconnaissance Drought Index [84]	RDI
Normalized Difference Vegetation Structure Index [70]	NDVSI
Modified Chlorophyll Absorption in Reflectance Index [70]	MCARI
Atmospherically Resistant Vegetation Index [85]	ARVI
Leaf Area Index [86]	LAI
Transformed Difference Vegetation Index [87]	TDVI
Renormalized Difference Vegetation Index [88]	RDVI
Visible Atmospherically Resistant Index [89]	VARI
Renormalized Difference Vegetation Index [88]	RDVI
Triangular Vegetation Index [90]	TVI
Modified Triangular Vegetation Index [89]	MTVI
Anthocyanin Reflectance Index [91]	ARI
Plant Senescence Reflectance Index [92]	PSRI
Red Green Ratio Index [93]	
Simple ratio of Red and NIR bands [94]	
Reduced Simple Ratio [94]	
Soil-Adjusted Total Vegetation Index [95]	SATVI
Total Vegetation Fractional Cover [95]	TVFC
Standardized Greenness-to-Cover Index [95]	GCI
Normalized Difference Moisture Index [75]	NDMI
Red and Short Wave Infra-Red [69]	RSWIR
Green and Short Wave Infra-Red [69]	GSWIR
Shortwave Infrared Soil Moisture Index [96]	SIMI
Normalized Difference Moisture Index [75]	NDMI
Normalized Difference Drought Index [71]	NDDI

Followed by the calculation of the remote sensing indices the altitude, slope and aspect of the study areas were also acquired by using SRTM imagery [30]. The calculated indices alongside the original Sentinel-2 bands and seasonal data (Tables 3.6 and 3.7) calculated from the date which the imagery were added to the dataset.

Table 3.6: Seasonal data used for the Iranian data

Season	Date range
spring	21 March to 21 June
summer	22 June to 22 September
autumn	23 September to 21 December
winter	22 December to 20 March

Table 3.7: Seasonal data used for the New Zealand data

Season	Date range
autumn	21 March to 21 June
winter	22 June to 22 September
spring	23 September to 21 December
summer	22 December to 20 March

The SPI-1, SPI-3 and SPI-6 data calculated previously which also coincided with the days the sentinel-2 imagery were captured were added to the dataset. Furthermore, to find new potential high quality features from the input data, genetic algorithm was used to undertake a feature construction procedure on the dataset. The algorithm created new features by using the NumPy- a scientific computing package- to conduct different operations such as subtraction, multiplication and division on different features [97]. The evaluation of the dataset was performed by using 10-fold cross validation [98]. Finally, the best features constructed were added to the final dataset alongside the old features.

As the number of input features in the dataset was quite large, a feature selection process was performed by using a genetic algorithm. This process was undertaken in order to remove features which did not contribute to the increase in the accuracy of the models. This genetic algorithm used a Randomforest classifier. The genetic algorithm also had the following parameters:

1. Crossover probability of 0.5

2. Mutation probability of 0.05
3. Population size of 590
4. Number of generations of 50

The feature selection process was repeated 20 times and the features which resulted in the highest performance were finally selected.The algorithm was created by using the DEAP (Distributed Evolutionary Algorithms in Python) library [99] which is implemented in Python. The features which contributed to the improvement of the models were kept in the datasets while the others were removed.

Furthermore, by using the TPOT (Tree-Based Pipeline Optimization Tool) Python library [100] optimized machine learning pipelines were created. TPOT is a wrapper implemented to be used with scikit-learn [101] and XGboost. Each machine learning pipeline operator available in TPOT corresponds to a machine learning algorithm implemented in scikit-learn or XGboost. By using the different machine learning pipeline operators TPOT creates different machine learning pipeline trees consisting of different operators. The operators in the trees are successively optimized by using an optimization algorithm implemented in DEAP. The performance of the altered pipelines are measured by evaluating the cross validation scores. The pipeline development process will continue until an end condition is met. The newly optimized models were then evaluated by using the testing dataset. The flowchart of the Sentinel-2 methodology can be seen in Figure 3.5.

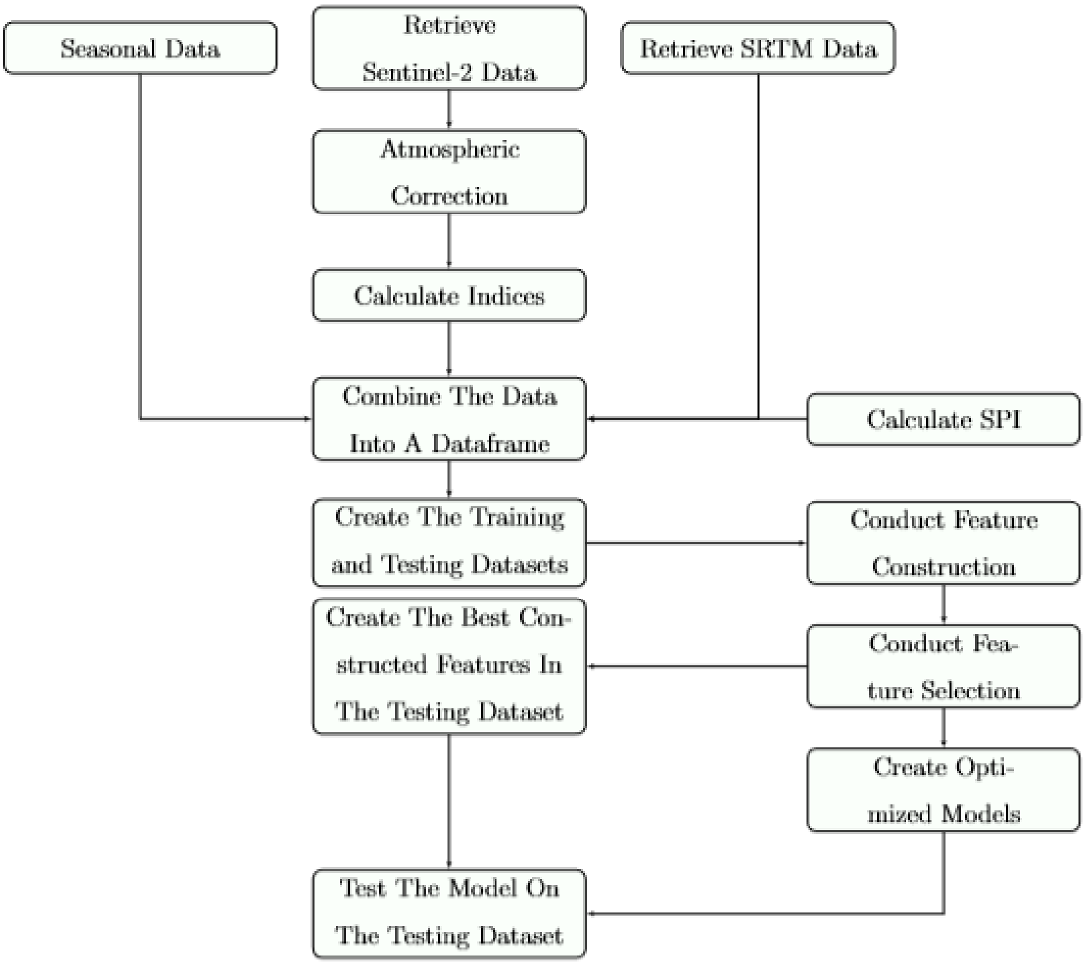

Figure 3.5: Sentinel-2 methodology flowchart

3.2 Sentinel-1 methodology

The second methodology for monitoring SPI-1, SPI-3 and SPI-6 values was developed using Sentinel-1 imagery. The imagery required for this methodology were retrieved by using the GEE Python API. GEE pre-processes Sentinel-1 imagery by using the SENTINEL-1 Toolbox. The pre-processing steps for the Sentinel-1 imagery are described in section 2.2.2 but further information can be found by visiting the GEE website [4].

Similar to the Sentinel-2 methodology, the Sentinel-1 data for pixels surrounding the weather station alongside the pixel where the weather station was located were

---

[4] https://developers.google.com/earth-engine/sentinel1

retrieved using GEE. This was performed by creating a circular buffer around the pixel where the weather station was located. The radius of the buffer was set to be 45 metres (Figure 3.3). This methodology assured that the data represented the GT more accurately.

.

The following values were retrieved by using Sentinel-1 imagery and were added to the Sentinel-1 datasets alongside SPI values which were calculated and coincided with the days the imagery were captured.

- VV
- VH
- Incidence angle
- Orbital direction data (Ascending or Descending)
- Normalized VV and VH values (equation 3.3)

$$Normalized\ Value = \frac{Current\ value - Maximum\ observed\ value}{Maximum\ observed\ value - Minimum\ observed\ value} \tag{3.3}$$

The altitude, slope and aspect of the areas of interest were also retrieved by using SRTM imagery alongside seasonal data (Tables 3.6 and 3.7) calculated by using the date of the captured Sentinel-1 imagery and were added to the datasets.

In addition to the SPI values calculated previously, the following input variable were added to the dataset:

- VV
- VH
- Incidence angle
- Altitude
- Slope
- Aspect
- Orbital direction
- spring
- summer
- autumn
- winter

Followed by the creation of the Sentinel-1 datasets the TPOT library was used to create optimized models for SPI-1, SPI-3 and SPI-6 by using the training dataset. The accuracy of the models were then measured by using 10-fold cross validation. To assess how the models performed on data not used in the training dataset the models were tested on the validation dataset. It was decided not to conduct feature selection by using a genetic algorithm as the number of features in the Sentinel-1 datasets were not high in comparison with the available number of samples. The flowchart of the Sentinel-1 methodology can be seen in Figure 3.6.

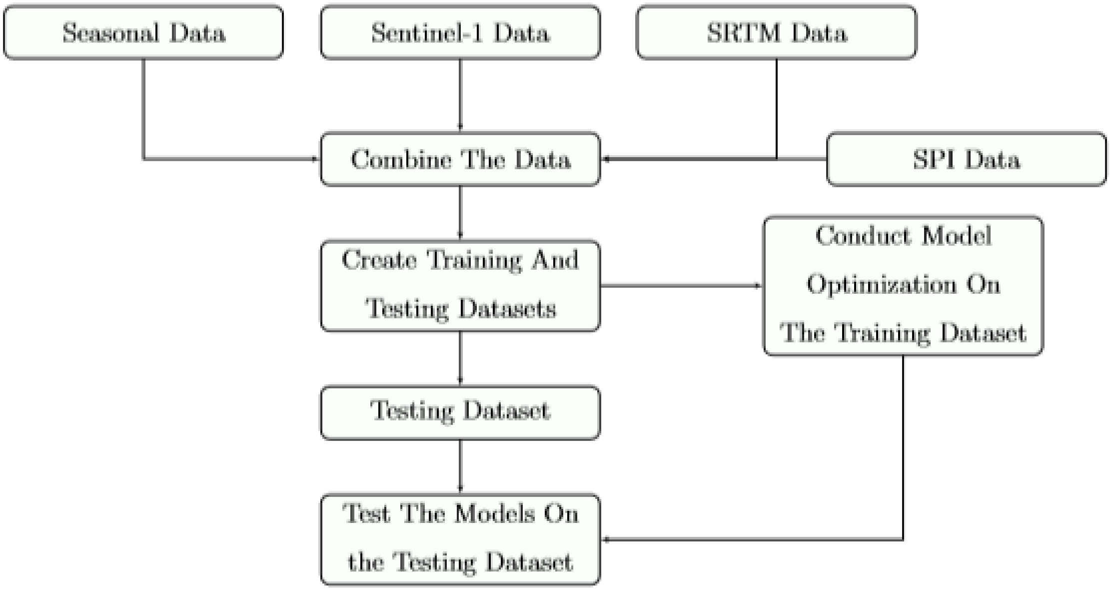

Figure 3.6: Sentinel-1 methodology flowchart

4

Sentinel-1 results and discussion

4.1 Sentinel-1 results

Table 4.1 demonstrates the results achieved by using the Sentinel-1 methodology. As can be seen the highest cross validation and testing scores are achieved when classifying SPI-1. The cross-validation scores for classifying SPI-3 and SPI-6 are the same but are slightly lower than SPI-1. In addition, the testing score accuracy decreases incrementally as the SPI values increase.

Table 4.1: Cross validation and testing scores achieved by using the Sentinel-1 methodology and the XGboost classifier

SPI	Cross validation score	Testing score
SPI-1	0.95	0.81
SPI-3	0.90	0.80
SPI-6	0.90	0.65

4.1.1 Correlation heatmap between Sentinel-1 input data and SPI values

Figure 4.1 shows the correlation heatmap between SPI values (SPI-1, SPI-3 and SPI-6) and each of the features used in the Sentinel-1 dataset described in section 3.2. The blue colours demonstrate negative correlation while the red colours represent positive correlation. Please note that the more saturated the colours are the higher the correlation is.

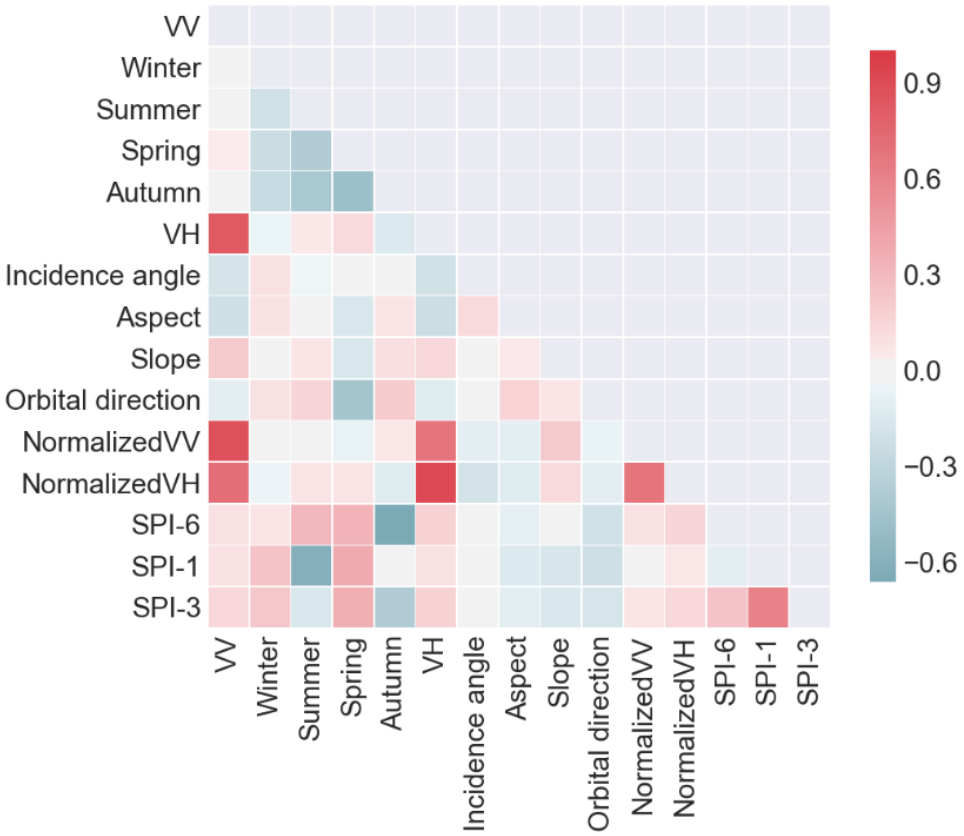

Figure 4.1: Correlation heatmap for Sentinel-1

4.2 Sentinel-1 discussion

As seen in Figure 4.1, the VV and VH bands of Sentinel-1 and the new features derived from them (normalized values) do not have a strong correlation with SPI values. In addition, with the exception of seasonal data none of the other features have a strong correlation with SPI values. For example, as it can be seen in Figure 4.1 the season of summer has a strong negative correlation with SPI-1 while a moderate positive correlation with SPI-6.

On the other hand, autumn has a strong negative correlation with SPI-6 and weak negative correlation with SPI-1. Furthermore, experiments were carried out to see how the VV and VH bands of Sentinel-1 affected the accuracy for classifying SPI values. It appears that the VV and VH values alone cannot be used to classify SPI values. However, by using these values in combination with other complementary data, SPI values can accurately be classified.

The data shown in Figure 4.1 clearly show that the season of summer has a strong negative correlation with SPI-1. This can be a result of the increase in temperature and decrease in precipitation which occurs in this season. This change in precipitation and temperature will result in more evaporation of soil moisture content and will cause more microwave energy to be absorbed by the soil (Figures 2.4 and 4.2).

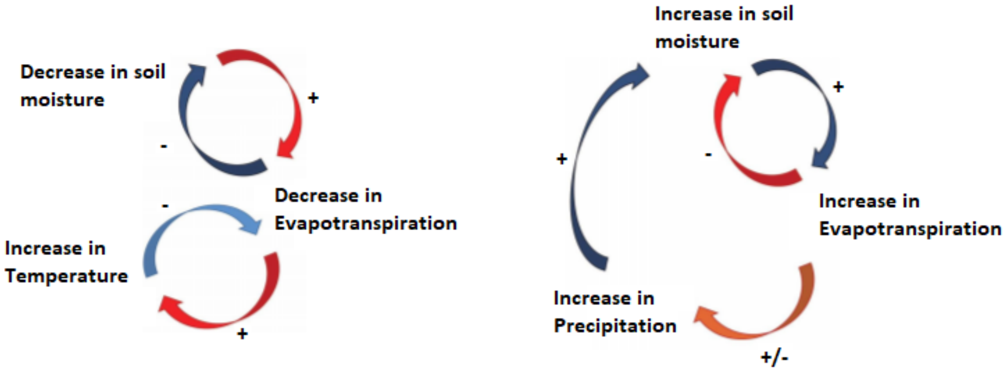

Figure 4.2: Processes contributing to change in soil moisture

There is a strong negative correlation between the season of autumn and SPI-6 and a moderate negative correlation with SPI-3 which can be due to the higher precipitation during this season. However, more research is required to further understand why this season is correlated with SPI-3 and SPI-6. A moderate positive correlation can also be seen with the season of spring and all the SPI values. This could be as a result of more precipitation and higher temperatures which cause more vegetation growth during this season. It appears that seasons that are associated with higher temperature levels have more impact on predicting short term SPI. Furthermore, the season of autumn which is associated with the decrease of temperature has an impact on predicting long term SPI.

The results obtained in this study (Table 4.1) shows that all the models have very high cross validation scores. However, when testing the models by using the testing dataset, the developed models seem to perform better for classifying SPI-1 and SPI-3 in comparison with SPI-6. This can be due to the fact that the VV and VH bands are sensitive to soil moisture and therefore, are not appropriate for monitoring vegetation health caused by long term drought. This can be confirmed as the cross validation score for the SPI-6 model is quite high while the testing accuracy is approximately 63 percent which shows that the model is not generalized well enough. The usefulness of Sentinel-1 imagery in approximating short term SPI values also confirms the reports [102, 103] on the success of Sentinel-1 imagery in monitoring soil moisture as SPI is designed for monitoring meteorological drought. The algorithm which was selected by TPOT and performed best on the Sentinel-1 datasets for classifying SPI values was the Extreme Gradient Boosting (XGboost) classifier (Table 4.1). This algorithm is based on the boosting machine learning methodology discussed in section 2.6.3 but uses more regularized model formalization in order to reduce the occurrence of overfitting and improving the performance of created models [104].

5

Sentinel-2 results and discussion

5.1 Sentinel-2 results

The results generated by using the feature construction procedure can be seen in the Tables below. The Tables 5.1, 5.2 and 5.3 contain the best features created by the genetic algorithm. The best constructed features were added to the Sentinel-2 datasets prior to the feature selection procedure. The majority of the constructed features were not selected by the feature selection process. However, the constructed features which were selected can be seen in Table 5.5. More information about the NumPy functions used during the feature construction process can be found at the NumPy and Scipy documentation webpages [1][2].

5.1.1 New constructed features for SPI-1

Table 5.1: Best constructed features for SPI-1

Number of constructed features	Constructed features for SPI-1
1	The remainder of the Red Green Ratio Index and the Plant Senescence Reflectance Index
2	The NumPy floor transformation for NDWI
3	The log1p transformation for ARI2
4	Multiplication of NIR and Red

---

[1] https://docs.scipy.org/doc/

[2] http://www.numpy.org

5.1.2 New constructed features for SPI-3

Table 5.2: Best constructed features for SPI-3

Number of constructed features	Constructed features for SPI-3
1	Subtraction of SWIR-1 and the Green band
2	The NumPy round transformation for slope
3	The NumPy sign transformation for aspect
4	The NumPy nanmin transformation for every row
5	The log1p transformation for SWIR-1

5.1.3 New constructed features for SPI-6

Table 5.3: Best constructed features for SPI-6

Number of constructed features	Constructed features for SPI-6
1	The NumPy trapz transformation for every row
2	The NumPy nansum transformation for every row
3	The NumPy Sin transformation for EVI
4	The NumPy diff transformation for every row

5.1.4 Feature selection results

As discussed previously the genetic algorithm which was used to conduct feature selection repeated 20 times and for 50 generations. In order to demonstrate this process 20 charts were generated for each of the different datasets. One of the generated charts created during the feature selection process can be seen in Figure 5.1. Finally, the best features were selected and added to the final datasets. The cross validation scores and percentage of features selected can be seen in Table 5.4.

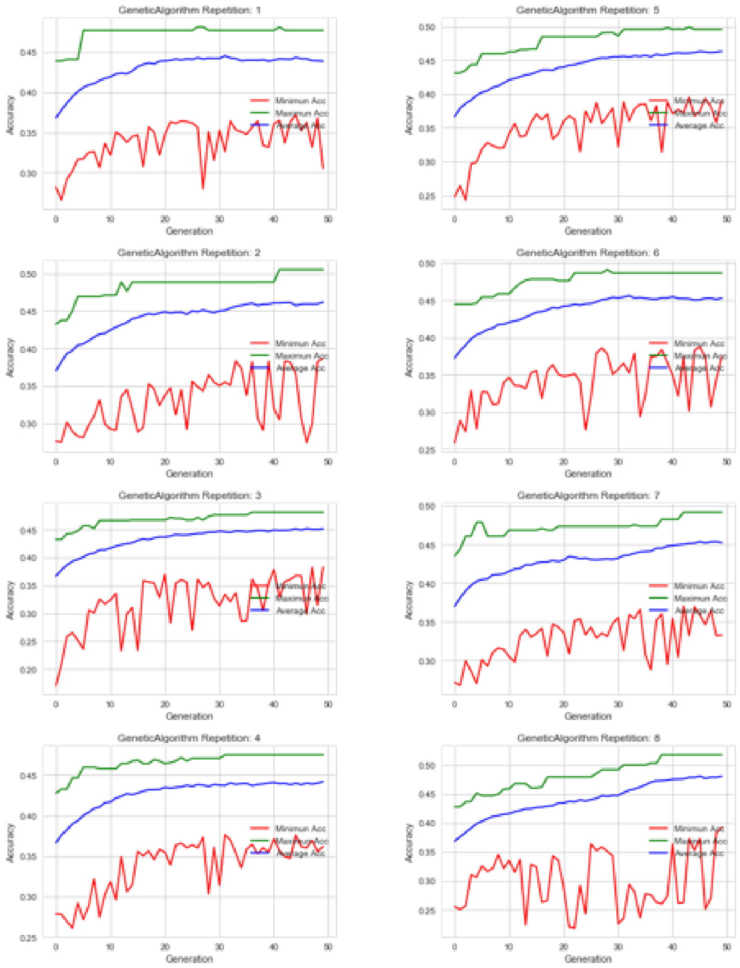

Figure 5.1: Chart generated by using the genetic algorithm for feature selection (SPI-1)

Table 5.4: Results generated following the feature selection process

SPI	Percentage of features selected	Cross validation score	Testing score
SPI-1	12.5	0.52	0.42
SPI-3	13	0.65	0.75
SPI-6	14.3	0.68	0.63

As seen in Table 5.4 the lowest testing score was achieved when predicting SPI-1 followed by SPI-6 and SPI-3. However, the highest cross validation score was achieved when predicting SPI-6 followed by SPI-3 and SPI-1.

5.1.5 The selected features for each of the SPI values

Table 5.5 shows the best features selected by the genetic algorithm for predicting SPI-1, SPI-3 and SPI-6 by using the Sentinel-2 datasets.

Table 5.5: Selected features of the Sentinel-2 datasets

Number of features	SPI-1	SPI-3	SPI-6
1	The NumPy log1p transformation for ARI2 (log1pARI2)	The NumPy round transformation for slope (Rounded slope)	The NumPy Sin transformation for EVI (sinEVI)
2	VARI	The NumPy log1p transformation for SWIR-1 (log1pSWIR1)	VSDI
3	Red	NDDI	NMDI
4	SWIR1	Tasseled Cap wetness	Tasseled Cap wetness
5	GVMI	Tasseled Cap greenness	Optimal soil adjusted vegetation index
6	BI	NDVSI	MTVI
7		ARVI	Triangular Vegetation Index
8		autumn	winter

5.1.6 Correlation heatmaps for selected Sentinel-2 features and SPI values

The heatmaps displayed in Figures 5.2, 5.3 and 5.4 demonstrate the correlation between SPI-1, SPI-3 and SPI-6 with the selected features (Table 5.5) used in the final Sentinel-2 datasets. The blue colours demonstrate negative correlation while the red colours represent positive correlation. The more saturated the colours are the higher the correlation is.

Correlation heatmap for selected Sentinel-2 features and SPI-1

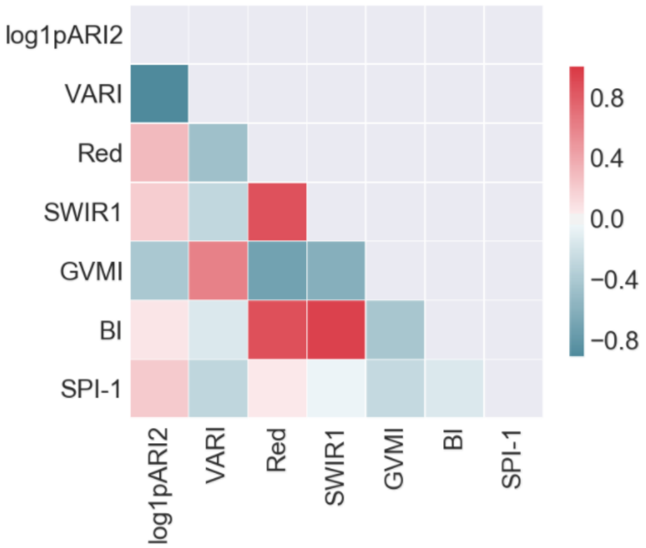

Figure 5.2: Correlation heatmap for selected Sentinel-2 features and SPI-1

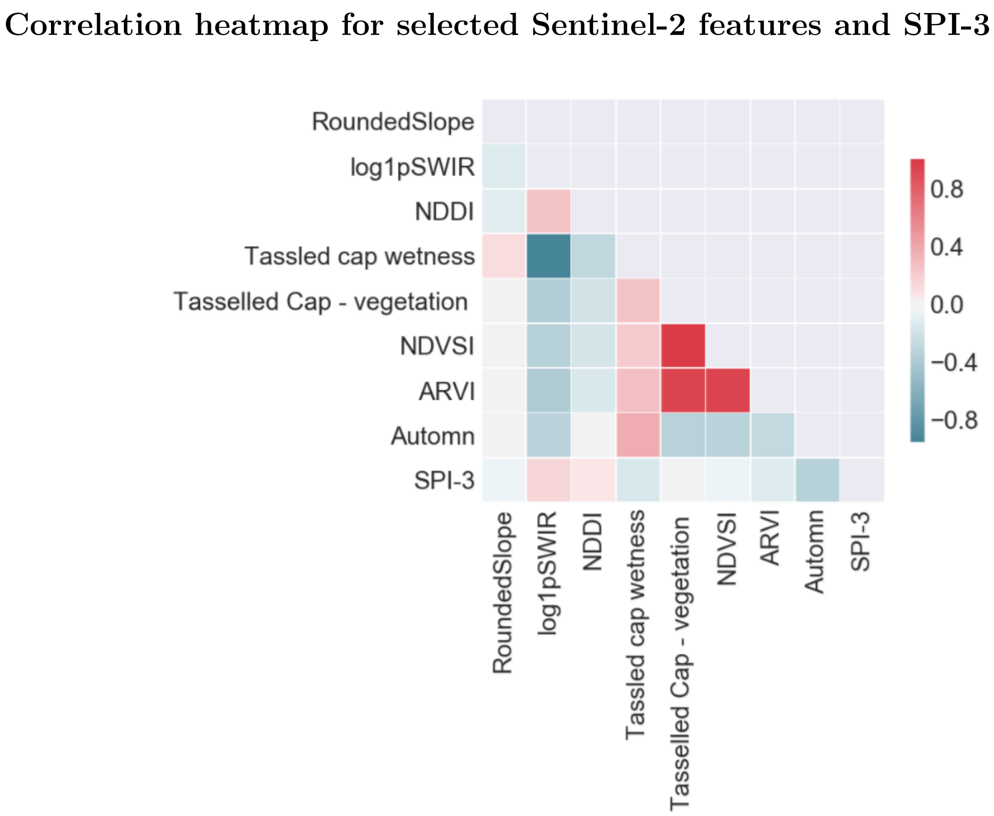
Correlation heatmap for selected Sentinel-2 features and SPI-3

Figure 5.3: Correlation heatmap for selected Sentinel-2 features and SPI-3

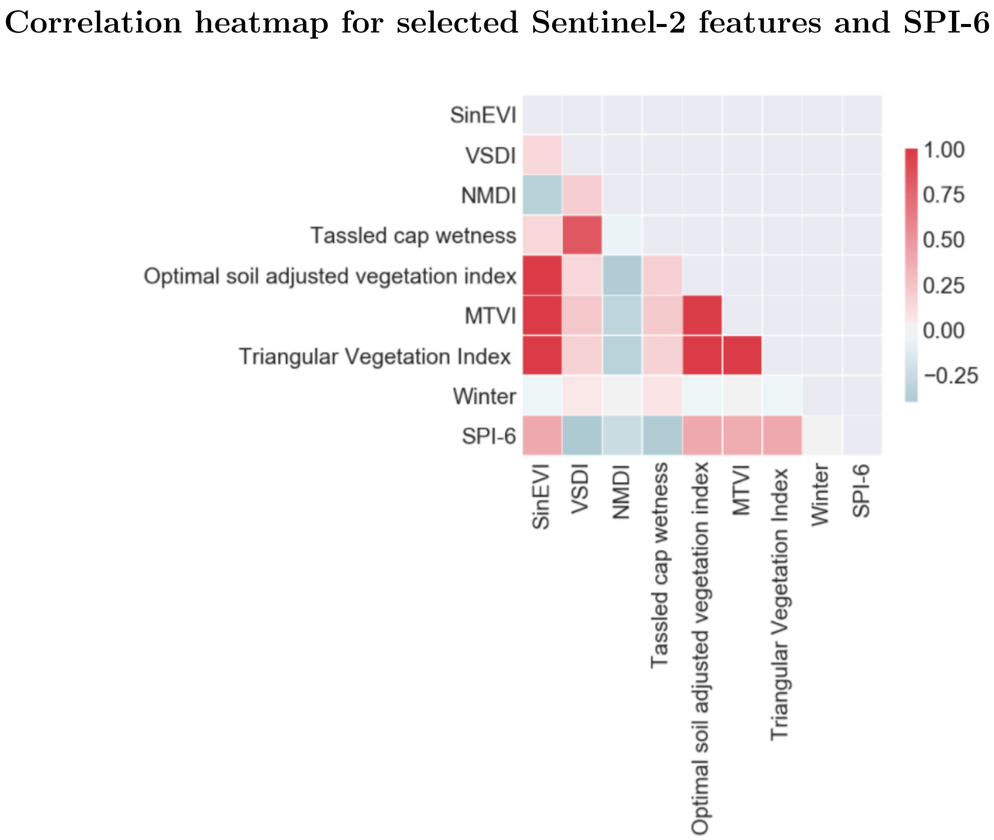
Correlation heatmap for selected Sentinel-2 features and SPI-6

Figure 5.4: Correlation heatmap for selected Sentinel-2 features and SPI-6

5.2 Sentinel-2 discussion

Followed by the calculation of the desired remote sensing indices shown in Table 3.5 by using the atmospherically corrected Sentinel-2 data retrieved from GEE the new features were constructed. The new features which resulted in the highest accuracy were obtained (Tables 5.1 5.2 and 5.3) which were added to the main dataset. Followed by adding the best constructed features to the main dataset, the genetic algorithm was used to select the best features while discarding others. In section 5.1.4 one of the charts obtained during the feature selection process can be seen. The following constructed features were selected by the genetic algorithm:

1. log1p ARI2 for classifying SPI-1
2. Rounded slope for classifying SPI-3
3. log1p SWIR1 for classifying SPI-3
4. sinEVI for classifying SPI-6

As mentioned above, two of the constructed and selected features are created by using the log1p transformation. The log1p function is used to transform the SWIR-1 and ARI2 indices. The ARI2 is a remote sensing index which is sensitive anthocyanins in plants. The values of ARI2 can help monitor and identify healthy and unhealthy plants in a geographical area. The SWIR-1 band has been proven to be sensitive to soil moisture [105] which can be the reason why it has been selected by the genetic algorithm. The purpose of the log1p function is to transform information to a natural logarithm of 1 + x.

Another constructed and selected feature for classifying SPI-3 is the rounded slope. The importance of slope can be explained because as the slope of an area increases, the amount of water which can be absorbed by the soil decreases (Figure 5.5)[3]. However, the amount of absorption highly depends on soil type as different soils absorb and hold different amounts of water. More research should be conducted to see how adding soil type information to the datasets could impact the performance of the models.

---

[3] https://deepgreenpermaculture.com/diy-instructions/how-to-build-a-french-drain/

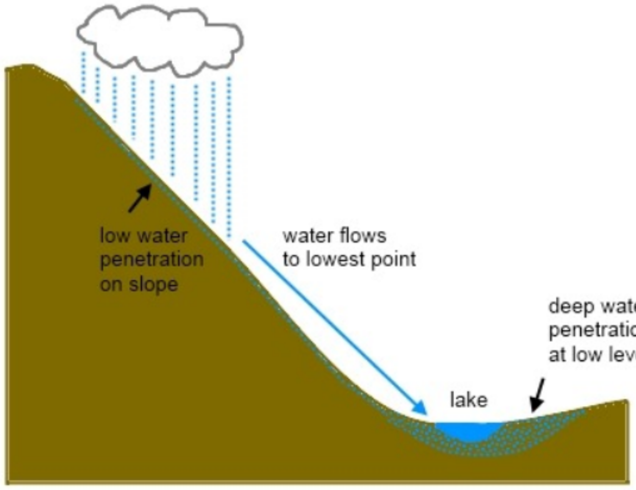

Figure 5.5: The impact of slope on water flow and soil water absorption

The only constructed feature which was selected for classifying SPI-6 was the sinEVI. By using the sine or cosine functions, or other forms of harmonic analysis, to transform vegetation indices such as EVI and NDVI useful information can be gained about an area of study such as the number of agricultural seasons or crop cycles [106]. In addition to the stated features other features were also selected and used in the final datasets which will be discussed in the following sections.

5.2.1 Selected features for SPI-1

The selected features for classifying SPI-1 other than the constructed features discussed previously are as follows:

1. Global Vegetation Moisture Index (GVMI): this index can be used for retrieving vegetation water content when the Leaf Area Index is equal or greater than 2. However, more research is required to see how this index performs in areas where vegetation is sparse (Leaf Area Index is less than 2) [107, 108] (Equation 5.1)

$$GVMI = \frac{(NIR + 0.1) - (SWIR + 0.02)}{(NIR + 0.1) + (SWIR + 0.02)} \tag{5.1}$$

2. Red and SWIR-1 bands: the Red band has been proven to be useful in discriminating vegetation slopes and the SWIR band is useful for discriminating

moisture content of soil and vegetation (Figure 5.6)[4]

3. Visible Atmospherically Resistant Index (VARI): this index is designed to measure vegetation in the visible portion of the spectrum, while mitigating illumination differences and atmospheric impacts
4. Brightness Index (BI): this index is calculated by summing all band reflectances to represent the overall reflectance strength of a target area

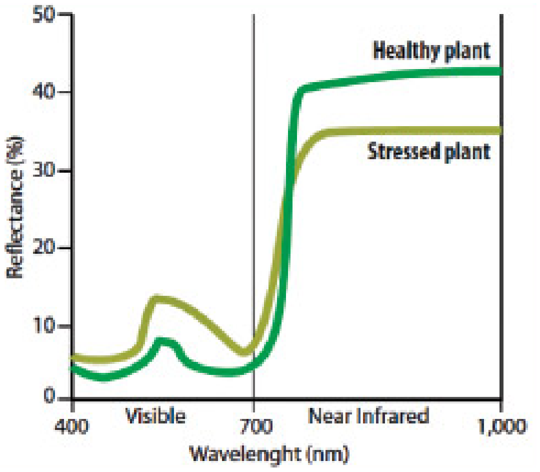

Figure 5.6: Change in reflectance in Red and NIR bands for healthy and unhealthy vegetation

A common theme of the chosen features for predicting SPI-1 is that they are mostly derived from the SWIR bands which are known to be sensitive to soil moisture and water content of the vegetation.

5.2.2 Selected features for SPI-3

As seen in Figure 5.3 none of the selected features have a strong correlation with SPI-3. However, the highest correlation is between SPI-3 and the season of autumn. This can be due to the fact that there are high precipitation levels during this season but more research is required to further understand the importance of this feature. Other than the season of autumn and the constructed features discussed previously the following features were selected by the genetic algorithm:

---

[4] http://mycoordinates.org/review-of-normalized-difference-vegetation-index-ndvi-as-an-indicator-of-drought/

1. Normalized Difference Vegetation Structure Index (NDVSI): this index is designed to capture crop vegetation structure and is based on the NIR band

2. Normalized Difference Drought Index (NDDI): NDDI is calculated by using the two well-known indices called NDVI and NDWI. NDVI is the most well-known remote sensing index which is used to monitor vegetation health and NDWI is often used to monitor the moisture content of vegetation

3. Tasseled Cap wetness and greenness: the Tasseled Cap transform formulas are used to create 'linear combinations' of spectral bands for satellite imagery. This behaviour of the Tasseled Cap formulas are similar to the Principal Components Analysis (PCA) which in machine learning is used for dimensional reduction. Both Tasseled Cap wetness and greenness were selected by the genetic algorithm for classifying SPI-3. The Tasseled Cap wetness index is useful for retrieving soil moisture information and the Tasseled Cap greenness index is useful for retrieving vegetating health information (Figures 5.7 and 5.8)[5]. Note that the axes of Figure 5.7 represent the spectral bands (bands four, five and six) of the Landsat satellite

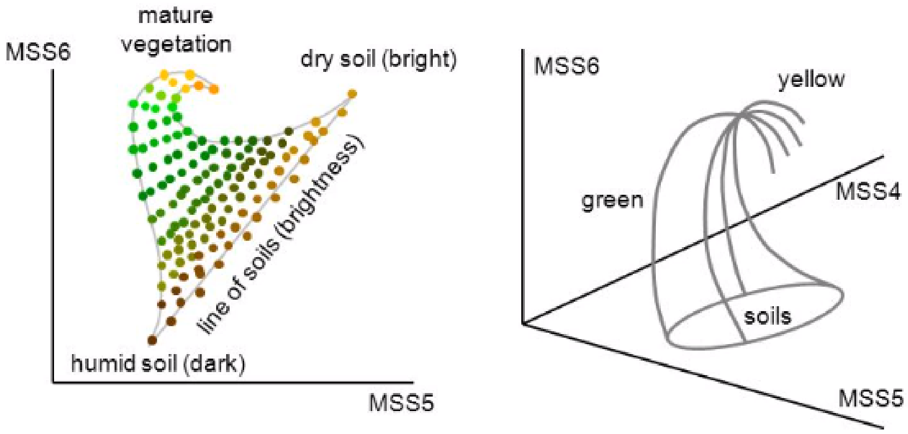

Figure 5.7: The variation of Multispectral Scanner (MSS) pixel positions corresponding to growing vegetation, as related to the Tasseled Cap transformation (Kauth and Thomas, 1976)

---

[5] http://geomatica.como.polimi.it/corsi/rs_ia/C10PCandTC.pptx.pdf

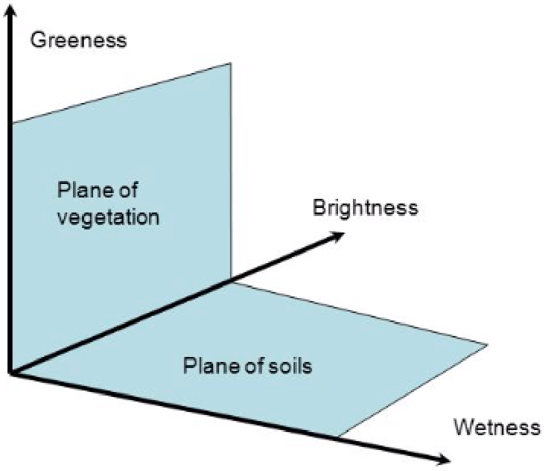

Figure 5.8: The planes and axes of the Tasseled Cap transformation

4. Atmospherically Resistant Vegetation Index (ARVI): this index is used to retrieve vegetation health information and has been proven to be useful in regions where atmospheric aerosol is high

Unlike the features selected for classifying SPI-1 which are based on SWIR data and are sensitive to soil and vegetation moisture, most indices selected for classifying SPI-3 measure the structure and health of vegetation in areas of interest.

5.2.3 Selected features for SPI-6

The selected indices for classifying SPI-6 other than sinEVI are as follows:

1. Visible and Shortwave Infrared Drought Index (VSDI): VSDI is calculated based on the difference between the moisture sensitive bands (SWIR and Red bands) and the moisture reference band (Blue). This index is often used to monitor agricultural drought. It is believed that this index has been selected by the genetic algorithm for classifying SPI-6 because long term SPI values impact vegetation health
2. Normalized Multi-band Drought Index (NMDI): this index is calculated by using the NIR and SWIR bands. The main purpose of this index is to monitor drought severity in areas with moderate amounts of vegetation coverage

3. Tasseled Cap wetness: as discussed previously this index was created based on the same concept as the PCA and is sensitive and useful in measuring soil moisture

4. Soil-Adjusted Total Vegetation Index (SATVI): this index is a modification of various vegetation indices such as NDVI and Soil-adjusted Vegetation Index (SAVI) and is used to monitor senescent vegetation. The selection of this index by the genetic algorithm shows that having information about senescent vegetation (Figure 5.9) can help the monitoring process of SPI-6


Dormant Foliated Senescent Flowering

Figure 5.9: Demonstration of different stages of the vegetation life cycle

5. Modified Triangular Vegetation Index (MTVI): this index modifies TVI in order to estimate LAI. This index is known to be used for monitoring leaf and canopy structures

6. Triangular Vegetation Index (TVI): Broge and Leblanc (2000) developed the triangular vegetation index (TVI) which is based on the area of a triangle with vertices at Green, Red and NIR wavelengths. This index is often used to monitor and approximate chlorophyll content and Leaf Area Index (LAI)

7. Winter: the selection of this feature shows that SPI-6 is sensitive and impacted by the amount of precipitation that occurs during the season of winter. However, further research should be conducted to better understand the relationship between this season and long term SPI

As seen above the majority of the selected features are indices used for monitoring LAI and vegetation health showing that indices which are associated with vegetation health and vigour are useful for monitoring SPI-6.

5.2.4 Feature selection outcomes

By comparing the selected features for different SPI values the following can be concluded:

1. SPI-1 values can be classified by using indices and bands which are sensitive to soil and vegetation moisture
2. SPI-3 and SPI-6 can be classified by using indices which are sensitive to vegetation health, structure and vigour
3. The seasons which seem to be the most important for classifying SPI-3 and SPI-6 are autumn and winter. This could be due to the fact that most of the precipitation occurs during these seasons. In addition, the season of summer has a significant correlation with SPI-1 values due to the higher temperatures occurring in this season

5.2.5 Final results of the Sentinel-2 methodology

Table 5.6 demonstrates the final results achieved by using the Sentinel-2 methodology after the optimization process. The results generated by using this methodology are considerably lower in comparison with the results generated by using the Sentinel-1 methodology with the exception of SPI-3.

Table 5.6: Accuracy of the Sentinel-2 methodology by using the Iran and New Zealand data

SPI	Cross validation score	Testing score
SPI-1	0.65	0.45
SPI-3	0.72	0.85
SPI-6	0.70	0.65

The accuracy of the model developed by using the Sentinel-2 methodology for classifying SPI-1 values was significantly lower in comparison with the results generated by using the Sentinel-1 methodology. This indicates the inability of the Sentinel-2 methodology for classifying SPI-1, even though most of the selected features chosen by the genetic algorithm were related to soil and vegetation moisture. In addition, the low prediction score of the Sentinel-2 methodology for predicting SPI-1 shows that this methodology is not suitable for monitoring SPI-1 which can be due to the fact that the indices calculated by using Sentinel-2 do not have a strong relationship or are not impacted by SPI-1 unlike SPI-3 and SPI-6.

The accuracy of this methodology for classifying SPI-3 had a lower cross validation score in comparison with the Sentinel-1 methodology but the testing score was better. The results generated for classifying SPI-6 were similar to the results achieved by using the Sentinel-1 methodology. In addition, the optimized machine learning pipelines created by using the TPOT library were much more complex in comparison with the pipelines developed for the Sentinel-1 methodology. This shows that it is much more complex to approximate SPI values by using the Sentinel-2 satellite imagery in comparison with sentinel-1 imagery. It seems that this methodology may be best suited for monitoring SPI-3. It appears that Sentinel-2 is more suitable for monitoring vegetation stress and health and more work should be undertaken to see how the use of Sentinel-2 imagery and machine learning algorithms could work for monitoring agricultural drought.

Although TPOT uses many algorithms from the Scikit learn library [101], it does not use Deep Neural Networks (DNN). Therefore, more research is required to investigate how the use DNN would impact the performance for classifying SPI by using the two methodologies. Also more research should be conducted to see how the combination of Sentinel-1 and 2 imagery will impact the performance for classifying SPI as well.

6

Conclusion

The creation of models by using the Sentinel-1 and Sentinel-2 methodologies achieved good results for classifying SPI-3 with an accuracy of approximately 80-85 percent on the testing dataset. However, the Sentinel-1 methodology had a significantly higher accuracy (80-82 percent) for classifying SPI-1 unlike the Sentinel-2 methodology which resulted in very poor results for classifying SPI-1 (45-50 percent). Both methodologies had a similar performance for classifying SPI-6 with an accuracy of 60-65 percent.

It is known that SPI is used for monitoring meteorological drought but longer SPI values also correspond to the occurrence of agricultural drought. This is due to the fact that the lack of precipitation for long periods of time results in change in vegetation greenness (health). This can be further validated by the fact that the majority of features selected (by using the genetic algorithm) for classifying SPI-6 are indices that are used to monitor vegetation health and vigour whereas the features selected for classifying SPI-1 are indices which are useful for monitoring soil and vegetation moisture. Although Sentinel-1 imagery has proven to be successful in monitoring short term SPI it requires to be used alongside complementary data such as SRTM and seasonal data to successfully approximate SPI values.

In addition, there has been research carried out by Park et al (2016) for monitoring SPI by using coarse satellite imagery from the Tropical Rainfall Measuring Mission (TRMM) and MODIS [39]. His study achieves very accurate results of approximately 90 percent when predicting SPI values which can be because Land Surface

Temperature (LST) and precipitation data have a high impact on predicting SPI values. Furthermore, his research shows that there is a strong relationship between remote sensing indices which are related to vegetation health and vigour and long-term SPI which is consistent with the work carried out in this research. Although the accuracy achieved by using Park et al's methodology is quite high, the SPI values predicted will have a low resolution due to the low resolution nature of the input data. However, the methodology developed during this research provides a way to predict SPI-1 and SPI-3 by using the Sentinel-1 methodology at a high resolution accurately and although, the Sentinel-2 methodology performs poorly for predicting SPI-1 and SPI-6 it can also be used to monitor SPI-3 at a high resolution accurately.

It can be concluded that the use of satellite imagery in combination with machine learning and cloud computing can provide a cost effective and simple solution for monitoring meteorological drought which is required for sustainable drought management which is a key objective for achieving the SDGs in particular SDG 15.3.

The use of the TPOT library allowed for the creation and optimization of machine learning pipelines easily but this library does not include deep learning algorithms such as Deep Neural Networks (DNN) at the moment. Therefore, further research is required to see how the use neural networks and DNN will impact the performance of the models for classifying SPI. In addition, more work is required to be undertaken in order to see how the two methodologies can be used for predicting agricultural drought and other drought indicators which incorporate evapotranspiration such as the Standardized Precipitation Evapotranspiration Index (SPEI). Finally, the usefulness of Sentinel-1 and Sentinel-2 data together for classifying SPI values should be studied as it may improve the SPI monitoring process.

Bibliography

[1] Thomas B McKee, Nolan J Doesken, John Kleist, et al. The relationship of drought frequency and duration to time scales. In *Proceedings of the 8th Conference on Applied Climatology*, volume 17, pages 179–183. American Meteorological Society Boston, MA, 1993.

[2] Colin P Kelley, Shahrzad Mohtadi, Mark A Cane, Richard Seager, and Yochanan Kushnir. Climate change in the fertile crescent and implications of the recent syrian drought. *Proceedings of the National Academy of Sciences*, 112(11):3241–3246, 2015.

[3] Habibollah Salami, Naser Shahnooshi, and Kenneth J Thomson. The economic impacts of drought on the economy of iran: An integration of linear programming and macroeconometric modelling approaches. *Ecological Economics*, 68(4):1032–1039, 2009.

[4] Jesse C Hillman and Alison KK Hillman. Mortality of wildlife in nairobi national park, during the drought of 1973–1974. *African Journal of Ecology*, 15(1):1–18, 1977.

[5] L Gudmundsson, FC Rego, M Rocha, and Sonia I Seneviratne. Predicting above normal wildfire activity in southern europe as a function of meteorological drought. *Environmental Research Letters*, 9(8):084008, 2014.

[6] Carla Stanke, Marko Kerac, Christel Prudhomme, Jolyon Medlock, and Virginia Murray. Health effects of drought: a systematic review of the evidence. *PLoS currents*, 5, 2013.

[7] Ana Russo, Célia M Gouveia, Patrícia Páscoa, Carlos C DaCamara, Pedro M Sousa, and Ricardo M Trigo. Assessing the role of drought events on wildfires in the iberian peninsula. *Agricultural and forest meteorology*, 237:50–59, 2017.

[8] Abd Al Salam Mohammed Mail. Desertification detected in the udhaim river basin, iraq based on spectral indices derived from remote sensing images. *Miscellanea Geographica*, 2017.

[9] Fredrik Charpentier Ljungqvist, Ulf Büntgen, Edward R Cook, Jan Esper, Dominik Fleitmann, Mary H Gagen, Elena García Bustamante, Jesús Fidel González-Rouco, Paul J Krusic, Jürg Luterbacher, et al. Summer temperature and drought co-variability across europe since 850 ce. In *EGU General Assembly Conference Abstracts*, volume 19, page 10561, 2017.

[10] Katherine Jean Seward, Daniel Taylor, and Cate Macinnis-Ng. *Drought Response Strategies and Sensitivity of Native Vegetation in the Auckland Region.* PhD thesis, University of Auckland, 2016.

[11] Austin R Coates, Philip E Dennison, Dar A Roberts, and Keely L Roth. Monitoring the impacts of severe drought on southern california chaparral species using hyperspectral and thermal infrared imagery. *Remote Sensing*, 7(11):14276–14291, 2015.

[12] Raushan Bokusheva, F Kogan, I Vitkovskaya, S Conradt, and M Batyrbayeva. Satellite-based vegetation health indices as a criteria for insuring against drought-related yield losses. *Agricultural and forest meteorology*, 220:200–206, 2016.

[13] Fawwaz T Ulaby, Richard K Moore, and Adrian K Fung. *Microwave Remote Sensing, Active and Passive, Volume I, Microwave Remote Sensing Fundamentals and Radiometry.* Reading, MA: Addison-Wesley, 1986.

[14] Zbyněk Malenovskỳ, Helmut Rott, Josef Cihlar, Michael E Schaepman, Glenda García-Santos, Richard Fernandes, and Michael Berger. Sentinels for science: Potential of sentinel-1,-2, and-3 missions for scientific observations of ocean, cryosphere, and land. *Remote Sensing of environment*, 120:91–101, 2012.

[15] Qi Gao, Mehrez Zribi, Maria Jose Escorihuela, and Nicolas Baghdadi. Soil moisture retrival from sentinel-1 and modis synergy. In *EGU General Assembly Conference Abstracts*, volume 19, page 8087, 2017.

[16] Nathan Torbick, Diya Chowdhury, William Salas, and Jiaguo Qi. Monitoring rice agriculture across myanmar using time series sentinel-1 assisted by landsat-8 and palsar-2. *Remote Sensing*, 9(2):119, 2017.

[17] Irena Hajnsek, Thomas Jagdhuber, Helmut Schon, and Konstantinos Panagiotis Papathanassiou. Potential of estimating soil moisture under vegetation cover by means of polsar. *IEEE Transactions on Geoscience and Remote Sensing*, 47(2):442–454, 2009.

[18] Safa Bousbih, Mehrez Zribi, Zohra Lili-Chabaane, Nicolas Baghdadi, Mohammad El Hajj, Qi Gao, and Bernard Mougenot. Potential of sentinel-1 radar data for the assessment of soil and cereal cover parameters. *Sensors*, 17(11):2617, 2017.

[19] Brian W Barrett, Edward Dwyer, and Pádraig Whelan. Soil moisture retrieval from active spaceborne microwave observations: An evaluation of current techniques. *Remote Sensing*, 1(3):210–242, 2009.

[20] Ferran Gascon, E Cadau, O Colin, B Hoersch, C Isola, B López Fernández, and P Martimort. Copernicus sentinel-2 mission: products, algorithms and cal/val. In *Earth Observing Systems XIX*, volume 9218, page 92181E. International Society for Optics and Photonics, 2014.

[21] Samuel N Goward and Darrel L Williams. Landsat and earth systems science: development of terrestrial monitoring. *Photogrammetric engineering and remote sensing*, 63(7):887–900, 1997.

[22] Maj-Liz Nordberg and Joakim Evertson. Monitoring change in mountainous dry-heath vegetation at a regional scaleusing multitemporal landsat tm data. *AMBIO: A Journal of the Human Environment*, 32(8):502–509, 2003.

[23] Christopher D Elvidge and Zhikang Chen. Comparison of broad-band and narrow-band red and near-infrared vegetation indices. *Remote sensing of environment*, 54(1):38–48, 1995.

[24] C Gomez, K Adeline, S Bacha, B Driessen, N Gorretta, P Lagacherie, JM Roger, and X Briottet. Sensitivity of clay content prediction to spectral configuration of vnir/swir imaging data, from multispectral to hyperspectral scenarios. *Remote Sensing of Environment*, 204:18–30, 2018.

[25] Amin Zargar, Rehan Sadiq, Bahman Naser, and Faisal I Khan. A review of drought indices. *Environmental Reviews*, 19(NA):333–349, 2011.

[26] Albert J. Peters, Elizabeth A. Walter-Shea, Lei Ji, Andrés Vina, Michael Hayes, and Mark D. Svoboda. Drought monitoring with ndvi-based standardized vegetation index. *Photogrammetric Engineering and Remote Sensing*, 68(1):71–75, 2002.

[27] Gyanesh Chander, Brian L Markham, and Dennis L Helder. Summary of current radiometric calibration coefficients for landsat mss, tm, etm+, and eo-1 ali sensors. *Remote sensing of environment*, 113(5):893–903, 2009.

[28] Gail Schmidt, Calli Jenkerson, Jeffrey Masek, Eric Vermote, and Feng Gao. Landsat ecosystem disturbance adaptive processing system (ledaps) algorithm description. Technical report, US Geological Survey, 2013.

[29] Andrii Shelestov, Mykola Lavreniuk, Nataliia Kussul, Alexei Novikov, and Sergii Skakun. Exploring google earth engine platform for big data processing: Classification of multi-temporal satellite imagery for crop mapping. *Frontiers in Earth Science*, 5:17, 2017.

[30] Tom G Farr, Paul A Rosen, Edward Caro, Robert Crippen, Riley Duren, Scott Hensley, Michael Kobrick, Mimi Paller, Ernesto Rodriguez, Ladislav

Roth, et al. The shuttle radar topography mission. *Reviews of geophysics*, 45(2), 2007.

[31] Tom G Farr and Mike Kobrick. Shuttle radar topography mission produces a wealth of data. *Eos, Transactions American Geophysical Union*, 81(48):583–585, 2000.

[32] Charles Warren Thornthwaite et al. Instructions and tables for computing potential evapotranspiration and the water balance. Technical report, Drexel Institute of Technology, Centerton, NJ (EUA). Laboratory of Climatology, 1957.

[33] Marvin Eli Jensen, Robert D Burman, and Rick G Allen. Evapotranspiration and irrigation water requirements. ASCE, 1990.

[34] Qiang Zhang, Chong-Yu Xu, and Zengxin Zhang. Observed changes of drought/wetness episodes in the pearl river basin, china, using the standardized precipitation index and aridity index. *Theoretical and Applied Climatology*, 98(1-2):89–99, 2009.

[35] Richard R Heim Jr. A review of twentieth-century drought indices used in the united states. *Bulletin of the American Meteorological Society*, 83(8):1149–1165, 2002.

[36] Ali Umran Komuscu. Using the spi to analyze spatial and temporal patterns of drought in turkey. *Drought Network News (1994-2001)*, page 49, 1999.

[37] J Zurovec, S Cadro, et al. The relationship between standardized precipitation index and yield reduction of significant agricultural crops in northeastern bosnia. In *Proceedings of the 22nd International Scientific-Expert Conference of Agriculture and Food Industry, Sarajevo, Bosnia and Herzegovina, 28 September-1 October, 2011*, pages 265–268. Ege University, Faculty of Agriculture, 2012.

[38] U Ma'rufah, R Hidayat, and I Prasasti. Analysis of relationship between meteorological and agricultural drought using standardized precipitation index and

vegetation health index. In *IOP Conference Series: Earth and Environmental Science*, volume 54, page 012008. IOP Publishing, 2017.

[39] Seonyoung Park, Jungho Im, Eunna Jang, and Jinyoung Rhee. Drought assessment and monitoring through blending of multi-sensor indices using machine learning approaches for different climate regions. *Agricultural and forest meteorology*, 216:157–169, 2016.

[40] Tao Ji, Guosheng Li, Hua Yang, Rui Liu, and Tairong He. Comprehensive drought index as an indicator for use in drought monitoring integrating multi-source remote sensing data: a case study covering the sichuan-chongqing region. *International Journal of Remote Sensing*, 39(3):786–809, 2018.

[41] Ahmad Fatehi Marj and Allard MJ Meijerink. Agricultural drought forecasting using satellite images, climate indices and artificial neural network. *International journal of remote sensing*, 32(24):9707–9719, 2011.

[42] Jesslyn F Brown, Brian D Wardlow, Tsegaye Tadesse, Michael J Hayes, and Bradley C Reed. The vegetation drought response index (vegdri): A new integrated approach for monitoring drought stress in vegetation. *GIScience & Remote Sensing*, 45(1):16–46, 2008.

[43] Tomislav Hengl, Jorge Mendes de Jesus, Gerard BM Heuvelink, Maria Ruiperez Gonzalez, Milan Kilibarda, Aleksandar Blagotić, Wei Shangguan, Marvin N Wright, Xiaoyuan Geng, Bernhard Bauer-Marschallinger, et al. Soilgrids250m: Global gridded soil information based on machine learning. *PloS one*, 12(2):e0169748, 2017.

[44] Carlos Gershenson. Artificial neural networks for beginners. *arXiv preprint cs/0308031*, 2003.

[45] Jochem Verrelst, Jordi Muñoz, Luis Alonso, Jesús Delegido, Juan Pablo Rivera, Gustavo Camps-Valls, and José Moreno. Machine learning regression algorithms for biophysical parameter retrieval: Opportunities for sentinel-2 and-3. *Remote Sensing of Environment*, 118:127–139, 2012.

[46] Robert E Schapire. A brief introduction to boosting. In *Ijcai*, volume 99, pages 1401–1406, 1999.

[47] Leo Breiman. Random forests. *Machine learning*, 45(1):5–32, 2001.

[48] Aleksandra Petrakova, Michael Affenzeller, and Galina Merkurjeva. Heterogeneous versus homogeneous machine learning ensembles. *Information Technology and Management Science*, 18(1):135–140, 2015.

[49] Mahesh Pal. Random forest classifier for remote sensing classification. *International Journal of Remote Sensing*, 26(1):217–222, 2005.

[50] Andy Liaw, Matthew Wiener, et al. Classification and regression by randomforest. *R news*, 2(3):18–22, 2002.

[51] Jerome H Friedman. Stochastic gradient boosting. *Computational Statistics & Data Analysis*, 38(4):367–378, 2002.

[52] Vahid Kazemi and Sullivan Josephine. One millisecond face alignment with an ensemble of regression trees. In *27th IEEE Conference on Computer Vision and Pattern Recognition, CVPR 2014, Columbus, United States, 23 June 2014 through 28 June 2014*, pages 1867–1874. IEEE Computer Society, 2014.

[53] Richard Bellman. *Dynamic programming*. Courier Corporation, 2013.

[54] Richard E Bellman. *Adaptive control processes: a guided tour*. Princeton university press, 2015.

[55] Svante Wold, Kim Esbensen, and Paul Geladi. Principal component analysis. *Chemometrics and intelligent laboratory systems*, 2(1-3):37–52, 1987.

[56] Pablo M Granitto, Cesare Furlanello, Franco Biasioli, and Flavia Gasperi. Recursive feature elimination with random forest for ptr-ms analysis of agroindustrial products. *Chemometrics and Intelligent Laboratory Systems*, 83(2):83–90, 2006.

[57] Riccardo Leardi, R Boggia, and M Terrile. Genetic algorithms as a strategy for feature selection. *Journal of chemometrics*, 6(5):267–281, 1992.

[58] Anil Jain and Douglas Zongker. Feature selection: Evaluation, application, and small sample performance. *IEEE transactions on pattern analysis and machine intelligence*, 19(2):153–158, 1997.

[59] Randal S Olson and Jason H Moore. Tpot: A tree-based pipeline optimization tool for automating machine learning. In *Workshop on Automatic Machine Learning*, pages 66–74, 2016.

[60] Fatemeh Rahimzadeh and Mojtaba Nassaji Zavareh. Effects of adjustment for non-climatic discontinuities on determination of temperature trends and variability over iran. *International Journal of Climatology*, 34(6):2079–2096, 2014.

[61] Sergio M Vicente-Serrano, Santiago Beguería, and Juan I López-Moreno. A multiscalar drought index sensitive to global warming: the standardized precipitation evapotranspiration index. *Journal of climate*, 23(7):1696–1718, 2010.

[62] Santiago Beguería, Sergio M Vicente-Serrano, Fergus Reig, and Borja Latorre. Standardized precipitation evapotranspiration index (spei) revisited: parameter fitting, evapotranspiration models, tools, datasets and drought monitoring. *International Journal of Climatology*, 34(10):3001–3023, 2014.

[63] Eric F Vermote, Didier Tanré, Jean L Deuze, Maurice Herman, and J-J Morcette. Second simulation of the satellite signal in the solar spectrum, 6s: An overview. *IEEE transactions on geoscience and remote sensing*, 35(3):675–686, 1997.

[64] Robin Timothy Wilson. Py6s: A python interface to the 6s radiative transfer model. *Computers & Geosciences*, 51(2):166, 2013.

[65] Loris Vescovo, Georg Wohlfahrt, Manuela Balzarolo, Sebastian Pilloni, Matteo Sottocornola, Mirco Rodeghiero, and Damiano Gianelle. New spectral vegetation indices based on the near-infrared shoulder wavelengths for remote detection of grassland phytomass. *International Journal of Remote Sensing*, 33(7):2178–2195, 2012.

[66] K Chandrasekar, MVR Sesha Sai, PS Roy, and RS Dwevedi. Land surface water index (lswi) response to rainfall and ndvi using the modis vegetation index product. *International Journal of Remote Sensing*, 31(15):3987–4005, 2010.

[67] Hongwei Zhang, Huailiang Chen, Rui Sun, Weidong Yu, Chunhui Zou, and Shuanghe Shen. The application of unified surface water capacity method in drought remote sensing monitoring. In *Remote Sensing for Agriculture, Ecosystems, and Hydrology XI*, volume 7472, page 74721M. International Society for Optics and Photonics, 2009.

[68] Ning Zhang, Yang Hong, Qiming Qin, and Lu Liu. Vsdi: a visible and shortwave infrared drought index for monitoring soil and vegetation moisture based on optical remote sensing. *International journal of remote sensing*, 34(13):4585–4609, 2013.

[69] Akhtar Ali Memon, Sher Muhammad, Said Rahman, and Mateeul Haq. Flood monitoring and damage assessment using water indices: A case study of pakistan flood-2012. *The Egyptian Journal of Remote Sensing and Space Science*, 18(1):99 – 106, 2015.

[70] Zhengwei Yang, Patrick Willis, and Rick Mueller. Impact of band-ratio enhanced awifs image to crop classification accuracy. *Pecora 17,—The Future of Land Imaging::: Going Operational Denver*, pages 18–20, 2008.

[71] Lingli Wang and John J Qu. Nmdi: A normalized multi-band drought index for monitoring soil and vegetation moisture with satellite remote sensing. *Geophysical Research Letters*, 34(20), 2007.

[72] Warren B Cohen. Response of vegetation indices to changes in three measures of leaf water stress. 1991.

[73] Edward P Glenn, Pamela L Nagler, and Alfredo R Huete. Vegetation index methods for estimating evapotranspiration by remote sensing. *Surveys in Geophysics*, 31(6):531–555, 2010.

[74] E Raymond Hunt, CST Daughtry, Jan UH Eitel, and Dan S Long. Remote sensing leaf chlorophyll content using a visible band index. *Agronomy journal*, 103(4):1090–1099, 2011.

[75] Suming Jin and Steven A Sader. Comparison of time series tasseled cap wetness and the normalized difference moisture index in detecting forest disturbances. *Remote Sensing of Environment*, 94(3):364–372, 2005.

[76] Takeshi Motohka, Kenlo Nishida Nasahara, Hiroyuki Oguma, and Satoshi Tsuchida. Applicability of green-red vegetation index for remote sensing of vegetation phenology. *Remote Sensing*, 2(10):2369–2387, 2010.

[77] John G Lyon, Ding Yuan, Ross S Lunetta, and Chris D Elvidge. A change detection experiment using vegetation indices. *Photogrammetric engineering and remote sensing*, 64(2):143–150, 1998.

[78] András Gulácsi and Ferenc Kovács. Drought monitoring with spectral indices calculated from modis satellite images in hungary. *Journal of Environmental Geography*, 8(3-4):11–20, 2015.

[79] Gaolong Zhu, Weimin Ju, JM Chen, and Yibo Liu. A novel moisture adjusted vegetation index (mavi) to reduce background reflectance and topographical effects on lai retrieval. *PloS one*, 9(7):e102560, 2014.

[80] C Jurgens. The modified normalized difference vegetation index (mndvi) a new index to determine frost damages in agriculture based on landsat tm data. *International Journal of Remote Sensing*, 18(17):3583–3594, 1997.

[81] Zhangyan Jiang, Alfredo R Huete, Kamel Didan, and Tomoaki Miura. Development of a two-band enhanced vegetation index without a blue band. *Remote sensing of environment*, 112(10):3833–3845, 2008.

[82] Muhammad Hasan Ali Baig, Lifu Zhang, Tong Shuai, and Qingxi Tong. Derivation of a tasselled cap transformation based on landsat 8 at-satellite reflectance. *Remote Sensing Letters*, 5(5):423–431, 2014.

[83] Leo Lymburner, Paul J Beggs, Carol R Jacobson, et al. Estimation of canopy-average surface-specific leaf area using landsat tm data. *Photogrammetric Engineering and Remote Sensing*, 66(2):183–192, 2000.

[84] T Thomas, RK Jaiswal, RV Galkate, and TR Nayak. Reconnaissance drought index based evaluation of meteorological drought characteristics in bundelkhand. *Procedia Technology*, 24:23–30, 2016.

[85] Yoram J Kaufman and Didier Tanre. Atmospherically resistant vegetation index (arvi) for eos-modis. *IEEE transactions on Geoscience and Remote Sensing*, 30(2):261–270, 1992.

[86] Eva Boegh, Henrik Soegaard, N Broge, CB Hasager, NO Jensen, Kirsten Schelde, and Anton Thomsen. Airborne multispectral data for quantifying leaf area index, nitrogen concentration, and photosynthetic efficiency in agriculture. *Remote sensing of Environment*, 81(2):179–193, 2002.

[87] A Bannari, H Asalhi, and PM Teillet. Transformed difference vegetation index (tdvi) for vegetation cover mapping. In *Geoscience and Remote Sensing Symposium, 2002. IGARSS'02. 2002 IEEE International*, volume 5, pages 3053–3055. IEEE, 2002.

[88] Jiali Shang, Jiangui Liu, Ted Huffman, Budong Qian, Elizabeth Pattey, Jinfei Wang, Ting Zhao, Xiaoyuan Geng, David Kroetsch, Taifeng Dong, et al. Estimating plant area index for monitoring crop growth dynamics using landsat-8 and rapideye images. *Journal of applied remote sensing*, 8(1):085196–085196, 2014.

[89] Driss Haboudane, John R Miller, Elizabeth Pattey, Pablo J Zarco-Tejada, and Ian B Strachan. Hyperspectral vegetation indices and novel algorithms for predicting green lai of crop canopies: Modeling and validation in the context of precision agriculture. *Remote sensing of environment*, 90(3):337–352, 2004.

[90] E Raymond Hunt, Paul C Doraiswamy, James E McMurtrey, Craig ST Daughtry, Eileen M Perry, and Bakhyt Akhmedov. A visible band index for remote sensing leaf chlorophyll content at the canopy scale. *International Journal of Applied Earth Observation and Geoinformation*, 21:103–112, 2013.

[91] Christian Hüttich, Ursula Gessner, Martin Herold, Ben J Strohbach, Michael Schmidt, Manfred Keil, and Stefan Dech. On the suitability of modis time series metrics to map vegetation types in dry savanna ecosystems: A case study in the kalahari of ne namibia. *Remote sensing*, 1(4):620–643, 2009.

[92] Michael J Hill. Vegetation index suites as indicators of vegetation state in grassland and savanna: An analysis with simulated sentinel 2 data for a north american transect. *Remote Sensing of Environment*, 137:94–111, 2013.

[93] JA Gamon and JS Surfus. Assessing leaf pigment content and activity with a reflectometer. *The New Phytologist*, 143(1):105–117, 1999.

[94] Pauline Stenberg, Miina Rautiainen, Terhikki Manninen, Pekka Voipio, Heikki Smolander, et al. Reduced simple ratio better than ndvi for estimating lai in finnish pine and spruce stands. 2004.

[95] Miguel L Villarreal, Laura M Norman, Steven Buckley, Cynthia SA Wallace, and Michelle A Coe. Multi-index time series monitoring of drought and fire effects on desert grasslands. *Remote Sensing of Environment*, 183:186–197, 2016.

[96] Rasmus Fensholt and Inge Sandholt. Derivation of a shortwave infrared water stress index from modis near-and shortwave infrared data in a semiarid environment. *Remote Sensing of Environment*, 87(1):111–121, 2003.

[97] Wes McKinney. *Python for data analysis: Data wrangling with Pandas, NumPy, and IPython.* " O'Reilly Media, Inc.", 2012.

[98] Ron Kohavi et al. A study of cross-validation and bootstrap for accuracy estimation and model selection. In *Ijcai*, volume 14, pages 1137–1145. Montreal, Canada, 1995.

[99] Félix-Antoine Fortin, François-Michel De Rainville, Marc-André Gardner, Marc Parizeau, and Christian Gagné. Deap: Evolutionary algorithms made easy. *Journal of Machine Learning Research*, 13(Jul):2171–2175, 2012.

[100] Randal S. Olson, Ryan J. Urbanowicz, Peter C. Andrews, Nicole A. Lavender, La Creis Kidd, and Jason H. Moore. *Applications of Evolutionary Computation: 19th European Conference, EvoApplications 2016, Porto, Portugal, March 30 – April 1, 2016, Proceedings, Part I*, chapter Automating Biomedical Data Science Through Tree-Based Pipeline Optimization, pages 123–137. Springer International Publishing, 2016.

[101] Fabian Pedregosa, Gaël Varoquaux, Alexandre Gramfort, Vincent Michel, Bertrand Thirion, Olivier Grisel, Mathieu Blondel, Peter Prettenhofer, Ron Weiss, Vincent Dubourg, et al. Scikit-learn: Machine learning in python. *Journal of machine learning research*, 12(Oct):2825–2830, 2011.

[102] Katarzyna Dabrowska-Zielinska, Maria Budzynska, Monika Tomaszewska, Alicja Malinska, Martyna Gatkowska, Maciej Bartold, and Iwona Malek. Assessment of carbon flux and soil moisture in wetlands applying sentinel-1 data. *Remote Sensing*, 8(9):756, 2016.

[103] Igor N Garkusha, Volodymyr V Hnatushenko, and Volodymyr V Vasyliev. Using sentinel-1 data for monitoring of soil moisture. In *Geoscience and Remote Sensing Symposium (IGARSS), 2017 IEEE International*, pages 1656–1659. IEEE, 2017.

[104] Tianqi Chen and Carlos Guestrin. Xgboost: A scalable tree boosting system. In *Proceedings of the 22nd acm sigkdd international conference on knowledge discovery and data mining*, pages 785–794. ACM, 2016.

[105] Ning Zhang, Yang Hong, Qiming Qin, and Lin Zhu. Evaluation of the visible and shortwave infrared drought index in china. *International Journal of Disaster Risk Science*, 4(2):68–76, 2013.

[106] Mark E Jakubauskas, David R Legates, Jude H Kastens, et al. Harmonic analysis of time-series avhrr ndvi data. *Photogrammetric engineering and remote sensing*, 67(4):461–470, 2001.

[107] Pietro Ceccato, Nadine Gobron, Stephane Flasse, Bernard Pinty, and Stefano Tarantola. Designing a spectral index to estimate vegetation water content

from remote sensing data: Part 1: Theoretical approach. *Remote sensing of environment*, 82(2-3):188–197, 2002.

[108] Pietro Ceccato, Stephane Flasse, and Jean-Marie Gregoire. Designing a spectral index to estimate vegetation water content from remote sensing data: Part 2. validation and applications. *Remote Sensing of Environment*, 82(2-3):198–207, 2002.